Technische Universität München
Fakultät für Physik

Master's Thesis

Determination of the Column Density in the KATRIN Beamline with Electrons from the Photo-Electric Source

Christoph Köhler

09. December 2019

Max-Planck-Institut für Physik
(Werner-Heisenberg-Institut)

Primary reviewer: Prof. Dr. Susanne Mertens
Secondary reviewer: Prof. Dr. Lothar Oberauer
Supervisor: Christian Karl

Declaration of Authorship

English:
I hereby declare that I am the sole author of this master's thesis and that it was written independently only using the cited external resources.

German:
Ich erkläre hiermit, dass die vorliegende Masterarbeit von mir selbstständig verfasst wurde und dass keine anderen als die angegebenen Quellen und Hilfsmittel benutzt wurden.

Christoph Köhler
Munich, 09.12.2019

Abstract

The Karlsruhe Tritium Neutrino (KATRIN) experiment currently provides the best limit on the effective electron antineutrino mass of all the experiments that use the direct method of observation to $m_\nu < 1.1\,\mathrm{eV}$ (90 % C.L.). It is designed to measure m_ν with a sensitivity of 200 meV (90 % C.L.) within 5 years of operation. To achieve this goal a strong reduction of statistical and systematical uncertainties is required. One important model parameter in the KATRIN experiment is the column density, that has to be determined with a precision of 0.2 %.

In this thesis different ways to obtain the column density were studied in detail. The most precise technique makes use of an angular resolved electron gun installed at the rear-end of the KATRIN beamline. In this thesis the analysis to infer the column density from the e-gun data was developed. To this end, a model of the KATRIN response function for e-gun electrons and the parameter inference based on the covariance matrix technique was implemented in the KATRIN analysis software Fitrium. This method was successfully applied for the first neutrino mass science run of KATRIN.

As the e-gun calibration is only performed on a weekly basis, means to determine the column density in between the e-gun calibrations during each beta-scan have to be found. To this end, the Beta Induced X-ray Spectrometry, Forward Beam Monitor and flowmeter sensor data was analyzed and a method to extract run-wise ρd values and uncertainties developed.

Furthermore, a study was performed to optimize the measurement time distribution of the column density determination with the photo-electron source. This thesis is concluded with an analysis of the first science run data, with a special focus on the correlation of the column density on the other parameters of interest, such as the neutrino mass and endpoint.

Contents

Chapter 1

Neutrinos in the Standard Model of particle physics and beyond

The neutrino is one of the greatest remaining mysteries in the world of particle physics. Its existence was first postulated theoretically. Being a lepton without electric charge and interacting only weakly, it took 30 years to be discovered in an experiment. Despite many discoveries ever since, the neutrino remains one of the least understood particles of the Standard Model. Among other open questions its absolute mass is still unknown.

This chapter is structured in the following way: In section 1.1 there is first given a brief summary of the history of the neutrino, followed by its theoretical description in the Standard Model in section 1.2. The recent discovery of neutrino oscillation is addressed in section 1.3 and the last section 1.4 is devoted to the neutrino mass determination.

1.1 Postulation and discovery

At the beginning of the 20^{th} century studying the β-decay of atomic nuclei J. Chadwick made an unexpected discovery. Unlike the discrete lines in α- and γ-decay, he observed a continuous energy spectrum for the emitted electrons [Cha14]. At this time the β-decay was thought to be a two-body decay with the emission of a proton and an electron. Both particles would always receive the same amount of energy in the decay, which stood in contrast to Chadwick's observation. A solution to this problem was proposed by W. Pauli in his famous letter to a group of physicists in 1930, where he postulated the existence of a neutral spin-$\frac{1}{2}$ particle that is emitted together with the electron in the β-decay [Pau30]. By sharing the energy released in the decay between this new particle and the electron the continuous spectrum could be understood. Further motivation for this postulation arose from the fact, that for angular momentum conservation additional spin was needed, which then would be provided by the new particle [Zub11].

After the discovery of the neutron only short time later E. Fermi was able to describe the β-decay in detail in his successful theory [Fer34]. The underlying reaction was now understood to be a three-body decay:

$$\mathrm{n} \rightarrow \mathrm{p}^{+} + \mathrm{e}^{-} + \bar{\nu}_e \tag{1.1}$$

More than 20 years after its postulation the existence of the neutrino was proven by Cowan and Reines in an experiment that was performed at Hanford in 1953 [CRH+56]. They used nuclear reactors as the source of an intense neutrino flux and observed the signal that arises from the reaction of an electron antineutrino with a proton, shown in eq. (1.2).

$$\bar{\nu}_e + \mathrm{p}^{+} \rightarrow \mathrm{e}^{+} + \mathrm{n} \tag{1.2}$$

Combining a large water tank with dissolved $CdCl_2$ with an additional liquid scintillator they could observe a very characteristic delayed pulse pair that is created by the reaction products. First, the positron annihilates with an electron resulting in the emission of 511 keV photons, which is then followed by the moderated neutron being captured on cadmium releasing a second pulse of photons

$$n + {}^{113}\mathrm{Cd} \rightarrow {}^{114}\mathrm{Cd} + \gamma. \tag{1.3}$$

The liquid scintillator detects both the photons from the positron annihilation and the neutron capture and hence the time-delayed spectrum could be studied in detail. To further confirm that the detected signals originated from reactor neutrinos interacting with the protons in the water tank, the signal rate was compared to the one expected from the reactor output. In this way, despite the large background of the experiment stemming from cosmic radiation, Cowan and Reines could conclude that they had detected neutrinos for the first time [CRH+56].

1.2 Standard Model description

The Standard Model of particle physics is a theory describing the interactions between fundamental forces and elementary particles [Pov+15]. It comprises three of the four known fundamental interactions: the strong, the weak and the electromagnetic force. It was developed by a large group of scientists in the second half of the 20th century and successfully predicted the existence of many new particles. However, the theory does not yet include the gravitational force and it cannot explain certain phenomena in particle physics, such as the observation of neutrino oscillation. This means that the Standard Model needs to be extended in order to cover all of the aspects of particle physics.

In the SM neutrinos are described as leptons without electric charge. Therefore they undergo only weak interactions. Experiments have proven that neutrinos violate parity. To explain this result the V–A theory of weak interaction was developed. Furthermore, the study of the charged pion decay implies that the electron neutrino is different from the muon neutrino [Pov+15]. The total number N_ν of light neutrinos was determined to be three by measuring the decay width of the Z^0 resonance [Zub11]. Neutrinos therefore exist in three different flavors that can be associated to each lepton family respectively:

$$\begin{pmatrix} \nu_e \\ e^- \end{pmatrix} \begin{pmatrix} \nu_\mu \\ \mu^- \end{pmatrix} \begin{pmatrix} \nu_\tau \\ \tau^- \end{pmatrix}$$

In the Standard Model description neutrinos are assumed to be massless. However in 1998 by discovering neutrino flavor oscillation it was shown that this assumption is not valid [FHI+98]. The fact that neutrinos have mass is to this date the only testable evidence of physics beyond the Standard Model and it makes the study of neutrino parameters so interesting [Pov+15].

1.3 Neutrino Oscillation

The first theoretical descriptions of neutrino oscillation were formulated in mid of the 20^{th} century by Pontecorvo, who predicted the possibility of neutrino-antineutrino oscillations [Pon68], and by Maki, Nakagawa and Sakata, who proposed a two flavor neutrino mixing

[MNS62]. The underlying requirement for these theories is that the neutrino flavor eigenstates differ from their mass eigenstates. The relation between them can be expressed via the so-called PMNS matrix

$$\begin{pmatrix} \nu_e \\ \nu_\mu \\ \nu_\tau \end{pmatrix} = \begin{pmatrix} U_{e1} & U_{e2} & U_{e3} \\ U_{\mu_1} & U_{\mu_2} & U_{\mu_3} \\ U_{\tau_1} & U_{\tau_2} & U_{\tau_3} \end{pmatrix} \begin{pmatrix} \nu_1 \\ \nu_2 \\ \nu_3 \end{pmatrix} \tag{1.4}$$

named after Pontecorvo, Maki, Nakagawa and Sakata. The matrix is parameterized by three mixing angles and one phase factor[1]. Assuming for simplicity the case of only two neutrino generations reduces eq. (1.4) to

$$\begin{pmatrix} \nu_e \\ \nu_\mu \end{pmatrix} = \begin{pmatrix} \cos\theta & \sin\theta \\ -\sin\theta & \cos\theta \end{pmatrix} \begin{pmatrix} \nu_1 \\ \nu_2 \end{pmatrix}. \tag{1.5}$$

In this case the mixing can be describe by only one parameter the mixing angle θ. Taking the electron neutrino as an example, it can now be expressed as a superposition of the mass eigenstates ν_1 and ν_2

$$|\nu_e\rangle = \cos\theta\,|\nu_1\rangle + \sin\theta\,|\nu_2\rangle \tag{1.6}$$

The oscillation probability of the electron neutrino can in this case be written as:

$$P\left(\nu_e \to \nu_\mu\right) = \sin^2(2\theta)\sin^2\left(\frac{\Delta m^2 L}{4E}\right) \tag{1.7}$$

One can see that the probability for oscillating into ν_μ depends on the mixing angle θ, the squared neutrino mass difference Δm^2, the distance the electron neutrino has traveled L and its energy E. By measuring this probability in experiments at different distances and neutrino energies the mixing angle and the squared neutrino mass difference can be determined.

First experimental indication for neutrino oscillation was found in the 1960s by R. Davis and his group at the Homestake experiment. Using a chlorine-based detector they measured the flux of solar electron neutrinos. The comparison with the theoretical prediction showed a significant deficit which soon became known as the solar neutrino problem [CDD+98].

In 1998 Super-Kamiokande was the first experiment to directly observe the oscillation of neutrinos, by studying the composition of the atmospheric neutrino flux and comparing it to the predicted value. The discrepancy between prediction and observation could only be explained by oscillation of ν_μ to ν_τ [FHI+98].

The second direct evidence for neutrino flavor transformation was found in the Sudbury Neutrino Observatory (SNO) experiment. Here, in contrast to the Homestake experiment they could additionally observe neutral current interactions and therefore prove, that the total flux of solar neutrinos, consisting of all three flavors matches the theoretical predictions. The solar neutrino problem could now be understood as the oscillation of ν_e to ν_μ or ν_τ [AAA+02].

1.4 Mass Determination

The phenomenon that neutrinos can oscillate implies that they have a non-zero mass. While the squared mass differences between the three mass eigenstates can be determined in oscillation experiments, the absolute value has to be obtained with other experiments.

[1] Two additional complex phases are needed in the case of Majorana neutrinos, discussed in section 1.4.2

1.4.1 Cosmology

One of the possible ways to access the neutrino mass is to study cosmological data. Because neutrinos have a high number density, they played an important role in the structure formation of the universe. After decoupling they were still highly relativistic particles and thus had a large free streaming length. The structures in the universe that we observe today were formed by small density fluctuations that grew in size due to gravitational clustering. The relativistic neutrinos acting as hot dark matter would mitigate this growth by washing out small scale structures. The strength of this effect depends on the neutrino mass. It is therefore possible to set an upper limit on the sum of neutrino mass eigenstates

$$m_{cos} = \sum_i m_i \tag{1.8}$$

by studying the cosmic microwave background anisotropy in combination with the observation of large-scale structures. A recent combined analysis using this method constraints the neutrino mass to

$$m_{cos} < 0.12\,\mathrm{eV} \tag{1.9}$$

as shown in [Agh+18]. This result, as well as the other limits on m_ν obtained from cosmological studies depend strongly on the underlying data set and are only valid within the ΛCDM concordance model.

1.4.2 Neutrinoless Double β-Decay

In double β-decay ($0\nu\beta\beta$), two neutrons decay simultaneously into two protons under emission of two electrons and two electron antineutrinos

$$2\mathrm{n} \rightarrow 2\mathrm{p} + 2e^- + 2\bar{\nu}_e. \tag{1.10}$$

If the neutrino is a Majorana particle, meaning that it is its own antiparticle, neutrinoless double β-decay ($0\nu\beta\beta$) is possible. Similar to the double β-decay ($2\nu\beta\beta$) two simultaneous β-decays are happening in the same nucleus. However, instead of creating two neutrinos, one virtual neutrino is exchanged inside the nucleus. This yields into a double β-decay where no neutrino is emitted

$$2\mathrm{n} \rightarrow 2\mathrm{p} + 2e^-. \tag{1.11}$$

The energy spectrum of the $0\nu\beta\beta$ would feature a sharp line at the endpoint because the two emitted electrons would receive the full decay energy [GP12]. The lifetime on the other hand depends on the effective Majorana neutrino mass

$$\mathrm{m}_{\beta\beta} = \left| \sum_k U_{\mathrm{ek}}^2 m_k \right| \tag{1.12}$$

which contains all three neutrino mass eigenvalues and the electron neutrino elements of the PMNS matrix. Possible cancellations can arise due to complex CP-violating phases. In addition the lifetime also depends on the nuclear matrix element of the decay, which therefore has to be known with high precision.

So far no direct observation of neutrinoless double β-decay could be made. The best upper limits on the neutrino mass could be determined in the GERDA experiment with ^{76}Ge to be $\mathrm{m}_{\beta\beta} < 0.15$ - $0.39\,\mathrm{eV}$ [Bar18] and in the KamLand-Zen experiment using ^{136}Xe to be $\mathrm{m}_{\beta\beta} < 0.09$ - $0.24\,\mathrm{eV}$ [Bar18].

1.4.3 Single β-Decay

One direct method to retrieve the absolute neutrino mass scale is the kinematic study of the single β-decay. The underlying reaction is

$$(A, Z) \rightarrow (A, Z+1)^{+} + e^{-} + \bar{\nu}_e + Q. \tag{1.13}$$

Here, in a nucleus (A,Z) a neutron decays into a proton resulting in a daughter nucleus $(A,Z+1)^{+}$ with an electron, an electron antineutrino and the surplus energy Q being emitted. In each decay Q is distributed in a way that the daughter nucleus receives a varying amount of recoil energy E_{rec} while the remaining energy, which is called the endpoint energy E_0

$$E_0 = Q - E_{\mathrm{rec}} = E + E_{\nu} \tag{1.14}$$

is being shared between the electron and the electron antineutrino. The electron receives the energy E and the electron antineutrino the energy E_{ν}. The maximal energy the electron can receive is therefore given by the difference between E_0 and the energy needed to create an electron antineutrino at rest. Studying the energy spectrum of the emitted electron one is able to retrieve information about the effective electron antineutrino mass

$$m_{\nu} = \sqrt{\sum_k |U_{\mathrm{ek}}^2| \cdot m_{\mathrm{k}}^2}, \tag{1.15}$$

which is defined as the incoherent sum of the squared neutrino mass eigenvalues m_{k}. The differential spectrum depending on the electron energy E is given by

$$\frac{\mathrm{d}\Gamma}{\mathrm{d}E} = C \cdot F(Z,E) \cdot p \cdot (E + m_{\mathrm{e}}) \cdot (E_0 - E) \cdot \sqrt{(E_0 - E)^2 - m_{\nu}^2} \cdot \Theta(E_0 - E - m_{\nu}). \tag{1.16}$$

In this equation the constant C is defined as

$$C = \frac{G_{\mathrm{F}}^2 \cdot \cos^2\theta_{\mathrm{C}}}{2\pi^3} \cdot |M_{\mathrm{nuc}}|^2. \tag{1.17}$$

It includes the Fermi constant G_{F}, the Cabbibo angle θ_{C} and the nuclear matrix element M_{nuc}. $F(Z,E)$ corresponds to the Fermi function

$$F(Z,E) = \frac{2\,\pi\,\eta}{1 - \exp(-2\,\pi\,\eta).} \tag{1.18}$$

and the momentum and mass of the electron are given by p and m_{e} [OW08; KBD+19].

Because the neutrino mass signal has only a small magnitude, the selection of the optimal β-isotope is of great importance. β-emitter with a low endpoint E_0 have a larger fraction of the total number of decays in the region near the endpoint. A short lifetime leads to a high activity and therefore to high statistics with a low amount of source material. Tritium with an endpoint of $\approx 18.6\,\mathrm{keV}$ and a half life of 12.3 yr satisfies both requirements and hence is used in the Mainz and Troitsk as well as in the KATRIN experiment [KBB+05; ABB+11; Ake+19].

Looking at the β-decay of tritium, the differential spectrum over the whole range of possible electron energies is shown in fig. 1.1a. According to eq. (1.16) the neutrino distorts the shape of the β-spectrum depending on the value of its the mass. The distortion near the endpoint for different neutrino masses is depicted in fig. 1.1b.

The current best limit on the electron antineutrino mass is

$$m_{\nu} < 1.1\,\mathrm{eV}\ (90\,\%\ \mathrm{C.L.})$$

and was measured by the KATRIN experiment in 2019 [AAA+19].

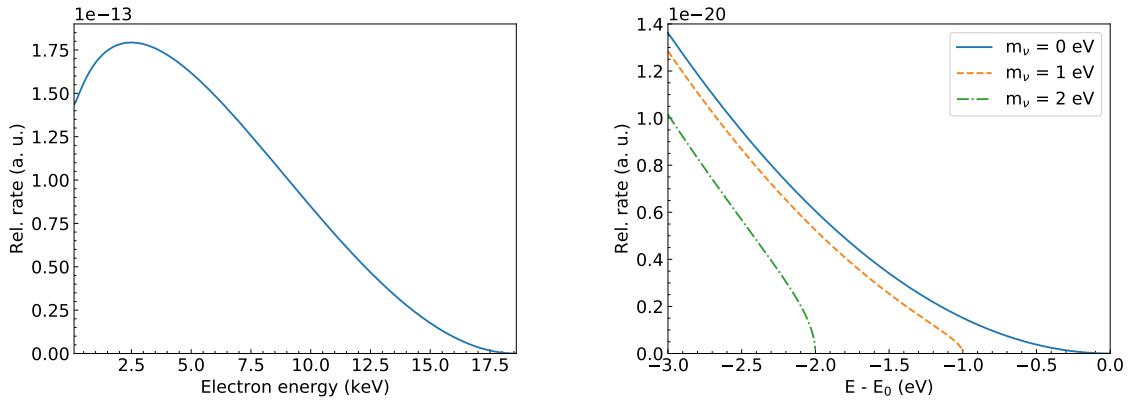

(a) Shape of the spectrum for the whole energy range.

(b) Impact of the neutrino mass on the spectral shape near the endpoint.

Figure 1.1: Differential spectrum of the tritium β-decay.

Chapter 2

The KATRIN Experiment

The KATRIN experiment currently provides the best limit on the neutrino mass of all the experiments that use the direct method of observation, see section 1.4.3. Its aim is to measure the neutrino mass with a sensitivity of 200 meV (90 % C.L.) probing the sub-eV neutrino mass scale. Like its predecessors the Mainz and Troitsk experiment it searches for distortions of the β-decay spectrum of tritium that are caused by a non-zero neutrino mass. The KATRIN experiment is located in Karlsruhe, where the Tritium Laboratory Karlsruhe (TLK) provides the necessary amount of tritium with high purity that is needed for the operation of the experiment. The goal of improving the ν-mass sensitivity by one order of magnitude in comparison with the Mainz and Troitsk experiment requires a reduction in statistical and systematic uncertainties by a factor of 100 [AAB+05].

In this chapter first the underlying measurement principle of the KATRIN experiment is described in section 2.1. It is followed by a description of the main experimental components that are needed to perform this high precision experiment in section 2.2. The last part, section 2.3, addresses the theoretical model that describes the measured integral β-spectrum.

2.1 MAC-E-Filter

To measure the energy spectrum of electrons emitted in tritium β-decay very precisely the KATRIN experiment uses a method called MAC-E-Filter (Magnetic Adiabatic Collimation in combination with an Elecrostatic Filter). This technique consists of a new type of spectrometer that was first introduced by [BPT80]. Having a good energy resolution and providing a high luminosity at the same time this measurement principle was soon identified as a promising candidate to enhance the search for the neutrino mass in direct experiments. It was redeveloped independently for this purpose by the Troitsk and Mainz experiment [LS85; PBB+92] and proved to be of great success.

The main tasks of the MAC-E-Filter consist of transforming the transversal energy $E_\perp$ of the electrons to energy in the parallel direction and providing an electric field that filters out all the electrons with energies below a certain threshold. This transformation is of great importance, since the electric field only acts in the longitudinal direction and therefore is not able to influence or determine the transversal part of the electron energy. The experimental components needed for this task together with an illustration of the electron momentum change are depicted in fig. 2.1. The β-electrons that are created in the tritium source are guided magnetically towards the spectrometer. Traveling with a cyclotron motion around the magnetic field lines they can enter the MAC-E-Filter with solid angles up to 2π. To transform their transversal energy the magnetic field acting upon them is continuously decreased from a maximum value $B_{\max}$ at the spectrometer entrance towards a minimal value B_{A} at the analyzing plane. This magnetic field gradient forces almost all of the transversal momentum

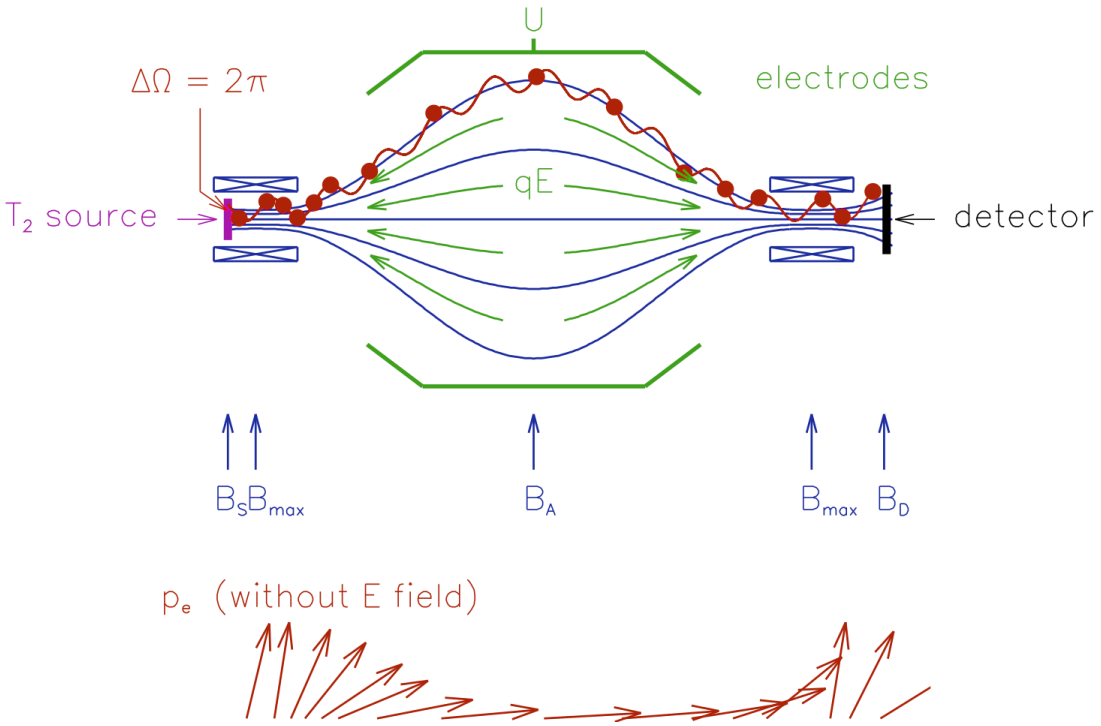

Figure 2.1: Illustration of the working principle of the MAC-E filter together with its experimental arrangement. Adapted from [AAB+05].

into the longitudinal direction. In case of adiabatic momentum transformation, which is valid here due to the slowly changing magnetic field, the magnetic moment μ stays constant:

$$\mu = \frac{E_\perp}{B} = \text{const.} \tag{2.1}$$

So by this technique the electrons that are created in the source by tritium decay are guided along the magnetic field lines through the spectrometer, where most of their transversal momentum is transformed into the longitudinal direction, and have to surpass a retarding potential in order to be reaccelerated and observed at the detector. Since for a given electric field only the electrons with an equal or higher energy can traverse the spectrometer, it acts as an integrating high-energy pass filter. Ideally it is desired to reduce all of the transversal electron energy. This is however not possible due to $B_\mathrm{A} > 0$. From eq. (2.1) follows that the MAC-E-Filter has a finite energy resolution which is given by

$$\frac{\Delta E}{E} = \frac{B_\mathrm{A}}{B_\mathrm{max}}. \tag{2.2}$$

In order to optimize the precision of the energy filter, the ratio between B_max and B_A should be as large as possible. At the same time, to guarantee the adiabaticity of the magnetic field the size of the spectrometer also has to become larger [AAB+05; KBD+19].

2.2 Experimental setup

The aim of the KATRIN experiment to measure the neutrino mass with a sensitivity of 200 meV requires a significant reduction of the experimental uncertainties. Using the fully developed technology of the MAC-E-Filter and being provided with highly purified tritium by the TLK, the experimental configuration consists of a setup which is 70 meters long and is shown in fig. 2.2. The tritium gas is injected continuously into the windowless source and pumped out at both ends to ensure a constant amount of gas being present. On the rear side of this source a section equipped with calibration devices is situated. The task to guide the emitted β-electrons towards the detector and to reduce the amount of residual gas in the beamline is fulfilled by the transport section. Following, the pre-spectrometer filters out the lower energetic β-electrons, to reduce the background that could be induced by them in the main spectrometer. The detector at the end of the beamline measures the rate of the electrons that surpass both spectrometers.

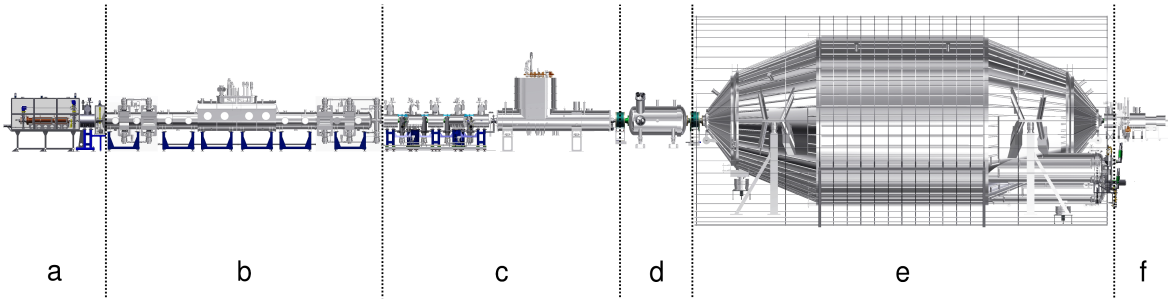

Figure 2.2: The experimental configuration of KATRIN can be separated in: a) the rear section, containing instruments for diagnostics, b) the windowless gaseous tritium source WGTS, c) the transport section, which consists of a differential and a cryogenic pumping section, d) the pre-spectrometer, e) the main spectrometer and f) the focal plane detector (FPD).

In the following the main experimental parts of KATRIN are described in more detail, starting with the components that are related to the creation and transport of the β-electrons, described in section 2.2.1. The energy filtering and detection of the electrons is addressed in section 2.2.2.

2.2.1 Source and transport section

As we have seen in section 1.4.3 the imprint of the neutrino mass on the β-spectrum is strongest in the region near the endpoint. However, only a tiny fraction of the total β-decays produces electrons with this high energies. To perform a neutrino mass measurement with low statistical uncertainty requires therefore a strong β-electron source.

In the following the three components of the KATRIN experiment that are directly related to the tritium source are described.

Rear Section

The rear section properly closes the WGTS on the rear side. For this task it contains a differential pumping section, that pumps the remaining tritium gas into the Outer Loop of

KATRIN. The rear end of the beamline is formed by the rear wall, a gold-plated stain-less steel disk, that absorbs the charged particles moving in this direction and ensures a well defined electrical potential over the full WGTS. Its location in the rear section is shown in fig. 2.3. A 5 mm wide hole in the wall enables the electrons from the photo-electron source, to pass into the beamline. By using an electromagnetic transport system, that includes steering coils in x- and y-direction, the electron beam is able to scan the whole flux tube area. With this mono-energetic and angular-selective beam of electrons a variety of calibration measurements is possible. One of the main tasks of the photo-electron source, in the following also called electron gun, is to determine the column density ρd of the tritium source with high precision. Furthermore the study of the transmission properties of the MAC-E-Filter as well as the determination of the energy loss function are from great importance and can be achieved using this electron beam. A second calibration device monitoring the WGTS properties is located near the rear wall. It uses Beta Induced X-ray Spectrometry (BIXS) to monitor the activity of the WGTS. The β-electrons from the tritium decay are absorbed at the rear wall and create X-rays through bremsstrahlung. Measuring the intensity of these photons allows the observation of activity fluctuations of the gas in the WGTS [AAB+05; Bab14; Beh16].

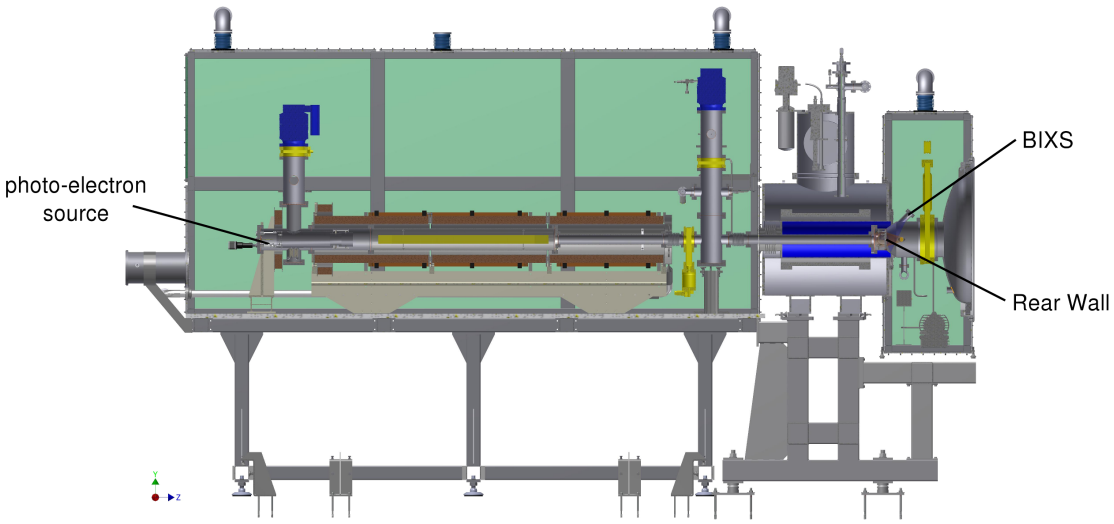

Figure 2.3: Illustration of the rear section setup. The rear wall terminates the beamline on this side. A small opening in the disk enables the electrons from the e-gun to pass into the beamline and with theses electrons dedicated calibration measurements can be performed. The BIXS detector monitors the activity of the sources by observing the emitted X-rays that are created when β-electrons reach the rear wall. Taken from [Bab14].

Windowless Gaseous Tritium Source

The tritium source of the KATRIN experiment consists of a windowless tube, where in the center molecular tritium gas is injected. The gas is pumped out at both ends to form a continuous circular flow of tritium. With this technique a constant gas column density of $5 \cdot 10^{17}\,\mathrm{cm}^{-2}$ can be achieved. In addition to providing this high column density the source

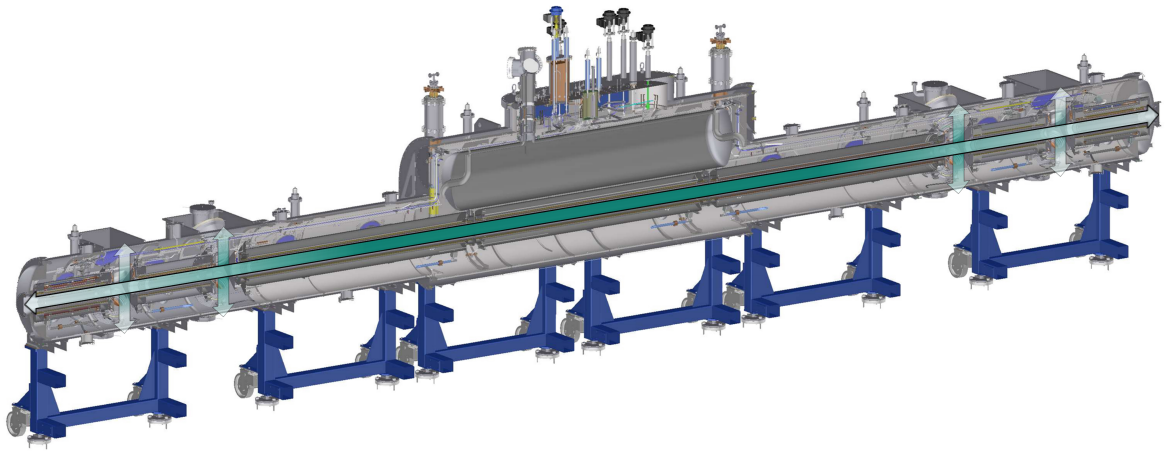

Figure 2.4: A cross-sectional view of the 11 m long windowless gaseous tritium source (WGTS). Tritium is injected in the center and flows out at both ends of the beamline, where turbo-molecular pumps transport the tritium back into the loop system. The density profile of the tritium gas is indicated with the green color. The β-electrons are guided magnetically to both sides, where they either enter the transport section or are absorbed at the rear wall. Taken from [Ha17].

needs to be stable on the per mille level.

Figure 2.4 displays the WGTS in an cross sectional view. The density of the tritium gas is indicated in the green color and allows the visualization of its flow inside the source. The starting point of this loop system is the supply of molecular tritium gas with a purity of $\epsilon_T > 95\,\%$ by the TLK [AAB+05]. Once the gas is injected, its composition can be monitored continuously using laser Raman spectroscopy (LARA). A cryostat keeps the source tube and the contained tritium gas at a stable temperature of 30 K. This mitigates the effect of Doppler broadening, which is due to the relative motion between the tritium molecules and the beamline axis, and lowers the chance of leaving the daughter molecule of the β-decay in a highly excited final state [Mar17]. The nominal column density of $5 \cdot 10^{17}\,\mathrm{cm}^{-2}$ is close to the optimal, maximal value, that is limited by the increasing probability of the electrons to undergo inelastic scattering. Raising ρd above the maximal value does not increase the signal strength anymore [AAB+05]. After injection, the bulk of the tritium gas is retracted at both ends of the source tube with four turbomolecular pumps and fed back into the loop cycle. The probability of creating β-electrons follows the density profile of the gas along the beamline axis. The electrons itself are emitted isotropically, with the pitch angle θ describing the direction of the electron momentum with respect to the magnet field.

With this setup the source of the KATRIN experiment can create about 10^{10} β-decay electrons per second. Using several superconducting magnets these electrons are guided along the magnetic field lines towards the detector and the rear wall, respectively. Because the β-electrons are emitted isotropically their path lengths inside the source differ in size. A longer path increases the probability to undergo inelastic scattering. It is therefore favorable to reject all electrons emitted with an angle above a certain value θ_{max}. This can be achieved by lowering the magnetic field inside the source according to the condition of magnetic

reflection, given in eq. (2.3).

$$\sin\theta_{\max} = \sqrt{\frac{B_S}{B_{\max}}} \tag{2.3}$$

To meet the KATRIN systematics budget the WGTS has to be operated with a stability on the per mille level in regard to the temperature and pressure inside the source. In addition the activity of the WGTS has to be monitored with high precision [Ha17; AAB+05].

Transport Section

After being created and selected by their angle the β-electrons enter the transport section. Here they are guided towards the entrance of the spectrometer using magnetic field coils. At the same time the flow of ions and neutral particles is drastically reduced. This is necessary due to the background that would be induced if these particles enter the spectrometer section. Between the tritium source and the end of the transport section the flow of tritium is reduced by 14 orders of magnitude. This is possible with a combination of a Differential Pumping Section (DPS), where the electrons enter first, and a Cryogenic Pumping Section (CPS), that connects to the spectrometer section. Their experimental setup is shown in fig. 2.5.

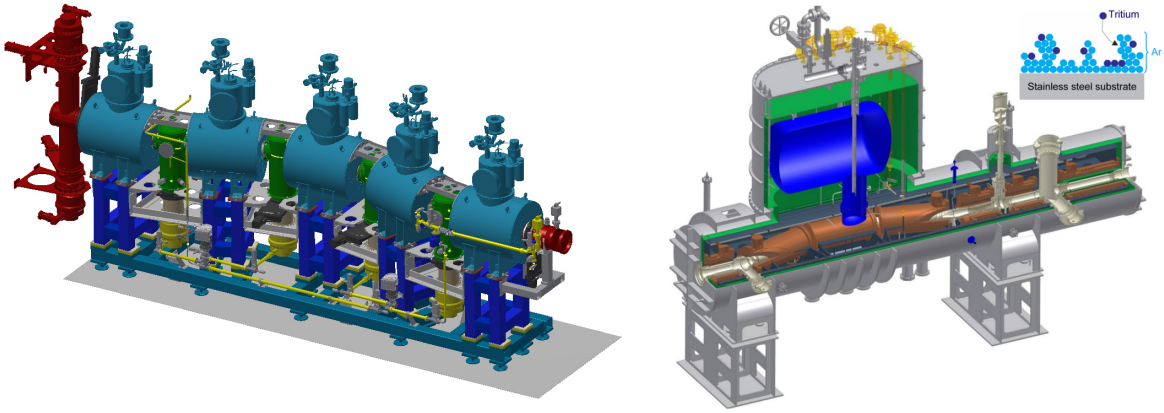

Figure 2.5: Illustrations of the two sub systems, that form the transport secion: The Differential Pumping Section (DPS) on the left and the Cryogenic Pumping Section (CPS) on the right. Images taken from [Jan15] (left) and from [Wal13] (right).

To guide the β-electrons the DPS exhibits five superconducting solenoids. Neutral particles are restraint to move in the forward direction by a 20° chicanery. This feature improves the pumping efficiency of the four turbomolecular pumps as well. In the DPS a gas-flow reduction by at least five orders of magnitude is achievable. To further prevent the flow of ions a ring electrode as well as electric dipole moments are installed, which will block these particles from moving forward.

At the entrance of the CPS, to complete the ion blocking, an additional ring electrode is installed. The reduction of the tritium flow by at least another seven orders of magnitude at the CPS is achieved using a different technique. With the implementation of seven superconducting magnets the beamline is tilted twice by 15°, forcing the remaining neutral particles to strike the beam tube. The inner surface of this tube is covered by a 3 K argon-frost layer, which absorbs the neutral particles [Are+18].

2.2.2 Spectrometer and detector section

The selection of the electron energies in KATRIN is achieved with two spectrometers that operate with the MAC-E-Filter principle. The first spectrometer, which is called the pre-spectrometer, filters out all the electrons with lower energy. By this, the flux of particles entering the main spectrometer is drastically reduced. This mitigates the background, that is created when the β-electrons hit remaining neutral gas particles in the spectrometer volume. The precise selection of the electron energy is performed in the main spectrometer. All the electrons that can surpass the retarding potential are collected and counted at the focal plane detector. The two spectrometers and the electron detector are described in the following in more detail.

Pre- and main spectrometer

The pre-spectrometer is located right after the CPS. In operation it rejects all electrons with an energy lower than a few hundred eV below the endpoint. This part of the β-spectrum carries almost no information about the neutrino mass. By applying this energy selection the flux of electrons is reduced, so that only a fraction of 10^{-6} of the initial particles can pass into the main spectrometer. The chance of exciting neutral residual gas atoms in the large main spectrometer volume is therefore mitigated. For this task of pre-filtering the pre-spectrometer does not require a good energy resolution. Accordingly the size of this component can be rather small.

Electrons that pass the first stage of the energy selection are guided by a 2 m long superconducting transport element towards the main spectrometer. This component of the KATRIN experiment consists of a 23.2 m long stainless-steel vessel with a diameter of 9.8 m. With this geometric parameters and using the MAC-E-Filter technique an energy resolution of 0.93 eV can be achieved. However, the large size of the vessel makes the main spectrometer vulnerable to the creation of background. To reduce the chance of electrons scattering on molecules in the spectrometer, a high vacuum of 10^{-11} mbar is applied. In addition an inner electrode system is installed at the inner surface of the vessel. The electrode system is held on a slightly more negative potential than the spectrometer walls. This rejects low energetic electrons originating from the wall, that fly in the direction of the flux tube.

The electrons that enter the main spectrometer are guided along the magnetic field lines through the volume. In the adiabatically changing magnetic field, that has its lowest value in the analyzing plane, the transverse energy of the electrons is transformed into the parallel direction. Depending on the retarding potential only a fraction of the electrons that entered the spectrometer have enough energy to overcome this threshold. After passing the potential, the electrons are reaccelerated towards the detector, where they are collected and counted [AAB+05; Are+18].

Focal Plane Detector

The focal plane detector of the KATRIN experiment consists of a multi-pixel silicon semiconductor detector with a high energy resolution. The experimental system where it is embedded can be seen in section 3.3. The electrons exiting the main spectrometer are passing into the FDP system, where they are guided by a local magnetic field. A post-acceleration electrode increases the energy of the β-electrons in order to detect them at the FPD in an energy region, where the background rate from the detector is reduced. With this elevated energy

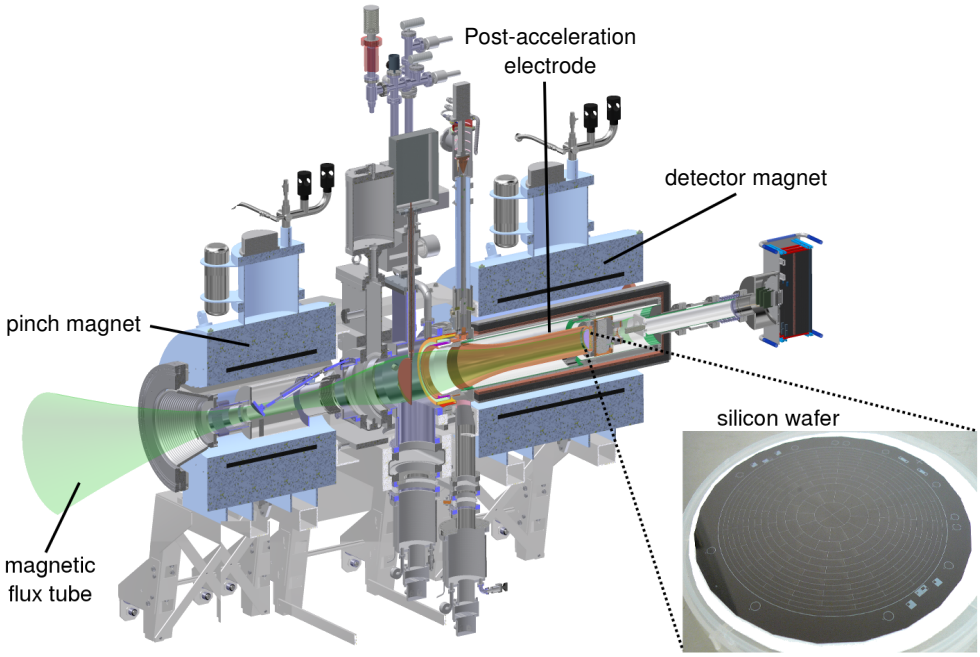

Figure 2.6: The experimental setup of the Focal Plane Detector. The flux tube is adjusted to the FPD geometry using an additional detector magnet. A post-acceleration electrode shifts the electron energy towards higher values. Adapted from [ABB+15; Wal13].

the electrons from the tritium decay are absorbed at the detector. The sensitiv area of the FPD with a diameter of 90 mm is divided into 148 pixels, where every pixel covers the same area of 44 mm^2. The pixels are arranged into 12 rings, each ring consisting of 12 pixels respectively. In the center of the detector the bulls eye with 4 additional pixels is situated. This structure allows the study of radial and axial inhomogenities, which could arise due to deviations in the electric or magnetic setup of the experiment.

For the neutrino mass measurement the rate of β-electrons is measured in dependence of the retarding potential, that is set at the main spectrometer. The FPD measures therefore an integral β-spectrum, from which the neutrino mass can be determined [ABB+15].

2.3 Model of the integral β-spectrum

Using the MAC-E-Filter method the KATRIN experiment measures an integral tritium spectrum. To determine the neutrino mass from this data the theoretical and experimental input, that leads to this spectrum, has to be known with high accuracy. The two components that contribute to this spectrum as well as the spectrum itself are addressed in the following.

2.3.1 Differential Decay Spectrum

The theoretical description of the β-decay, that was already addressed in section 1.4.3, has to be specified to include the properties of the KATRIN tritium source. The usage of molecular tritium leads to the possible excitation of rotational and vibrational final states in the β-

decay. Therefore the energy of the neutrino has to be adjusted by the energy V_f of each final state:

$$E_0 - E \rightarrow E_0 - V_f - E = \epsilon_f \tag{2.4}$$

Additionally, the decay spectrum has to be summed over each final state f and weighted by the probability that this state occurs. The differential decay spectrum can then be written as

$$\frac{\mathrm{d}\Gamma}{\mathrm{d}E} = C \cdot F(Z,E) \cdot p \cdot (E + m_\mathrm{e}) \cdot \sum_f \cdot P_f \cdot \epsilon_f \cdot \sqrt{\epsilon_f^2 - m_\nu^2} \cdot \Theta(\epsilon_f - m_\nu). \tag{2.5}$$

Another effect that has to be taken into account is the thermal motion of the tritium molecules. This leads to a broadening of the differential spectrum by the Doppler effect. It can be addressed by convolving the differential spectrum with a broadening function g:

$$\frac{\mathrm{d}\Gamma}{\mathrm{d}E} = \int_{-\infty}^{\infty} g(E_\mathrm{cms}, E_\mathrm{lab}) \, \frac{\mathrm{d}\Gamma}{\mathrm{d}E}\,(E_\mathrm{cms}) \, \mathrm{d}E_\mathrm{cms}. \tag{2.6}$$

Here, E_cms is kinetic energy of the electrons in the center-of-mass system and E_lab is the energy in the laboratory frame [KBD+19].

2.3.2 Response function

The second contribution, that has to be known with high precision, is the response function of the experiment. It describes how the β-electrons propagate from the source to the detector. In KATRIN, the main causes for this response are the energy selection with the MAC-E-Filter and the energy loss of electrons due to scattering in the source.

The probability of an electron with energy E to pass the spectrometer with the retarding potential U can be described by the so-called transmission function $T(E, qU)$ [AAB+05]. For the present isotropic electron source it is given by

$$T(E,qU) = \begin{cases} 0 & E - qU < 0 \\ \dfrac{1 - \sqrt{1 - \frac{E-qU}{E} \cdot \frac{B_\mathrm{S}}{B_\mathrm{A}} \frac{2}{\gamma+1}}}{1 - \sqrt{1 - \frac{\Delta E}{E} \cdot \frac{B_\mathrm{S}}{B_\mathrm{A}}}} & 0 \leq E - qU \leq \Delta E \\ 1 & E - qU > \Delta E \end{cases}. \tag{2.7}$$

Here, for the relativistic description of the electrons, the gamma factor $\gamma = \frac{E}{m_\mathrm{e}} + 1$ is used. The relation between the transmission probability and the electron energy is shown in fig. 2.7a for the nominal KATRIN settings.

The energy loss of the electrons traversing the source can be described using an energy loss function $f(\epsilon)$, that gives the probability of a certain energy loss ϵ in a scattering reaction, in combination with the function $\mathrm{P}_s(\theta)$ that describes the likelihood that the electron scatters. In the WGTS the electrons can undergo elastic and inelastic scattering processes. Since only the latter result in a mentionable energy loss, the contribution of elastic scattering is neglected.

The energy loss function is parameterized as

$$f(\epsilon) = \begin{cases} A_1 \cdot \exp\left(-2\left(\frac{\epsilon - \epsilon_1}{\omega_1}\right)^2\right) & \epsilon < \epsilon_c \\ A_2 \cdot \frac{\omega_2^2}{\omega_2^2 \, + \, 4(\epsilon \, - \, \epsilon_2)^2} & \epsilon \geq \epsilon_c \end{cases}, \tag{2.8}$$

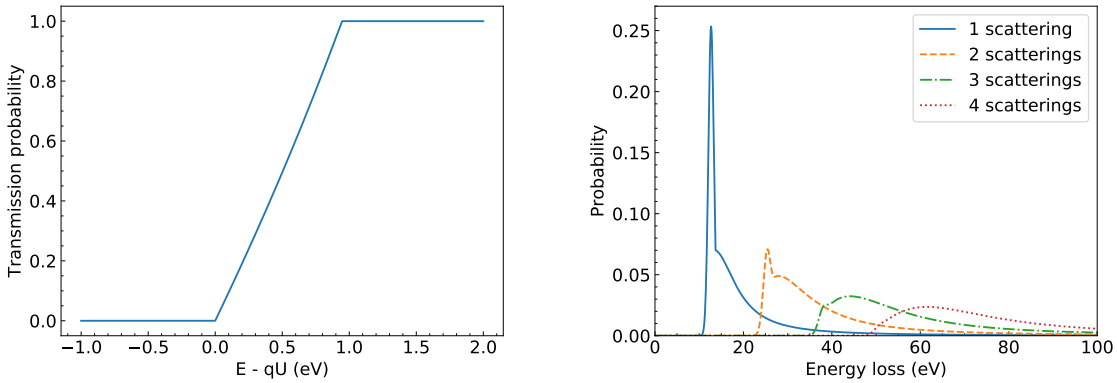

(a) Transmission function.

(b) Energy loss function.

Figure 2.7: Transmission function of the KATRIN experiment for nominal settings and the energy loss function shown for the first four scatterings.

with a Gaussian part describing the losses from excitation processes and a Lorentzian part for the losses originating from the ionization of tritium molecules [KBD+19]. For an electron, that scatters only once, this function returns accurately the energy loss spectrum of this event. In case the electron scatters N-times, the energy loss function has to be convolved (N-1)-times with itself. This is shown in fig. 2.7b on the right for up to four scatterings. If the electrons exit the source without scattering the energy loss function simply becomes $f_0(\epsilon) = \delta(\epsilon)$.

The probability for the electrons to undergo inelastic scattering depends on the position z in the source, where they were created. This relation can be expressed with an effective column density $\mathcal{N}_{\text{eff}}$, that the electrons see on their way through the WGTS. In addition to the position, $\mathcal{N}_{\text{eff}}$ includes the density distribution of ρd as well as the starting angle of the electrons:

$$\mathcal{N}_{\text{eff}}(z,\theta) = \frac{1}{cos(\theta)} \cdot \int_{z}^{L/2} \rho(z')\ \mathrm{d}z'. \tag{2.9}$$

Furthermore, the scattering probability also depends on the inelastic cross section σ_{inel} [Liu87], that is given by

$$\sigma_{\text{inel}}(T) = \frac{4\pi a_0^2}{T/R}\left[1.5363\ \ln\left(\frac{4.72\ T}{R}\right) - 0.0097\right]. \tag{2.10}$$

It can be seen, that σ_{inel} depends on the non-relativistic kinetic energy T of the electrons. The constants a_0 and R are the Bohr radius and the Rydberg energy respectively. Depending on the position and the angle of the electron, the probability to scatter inelastic is determined to be

$$P_{\text{inel,N}}(z,\theta) = \frac{(\mathcal{N}_{\text{eff}}(z,\theta)\cdot\sigma_{\text{inel}})^N}{N!} \cdot \exp(-\mathcal{N}_{\text{eff}}(z,\theta)\cdot\sigma_{\text{inel}}). \tag{2.11}$$

Looking at the case of multiple scattering and taking the mean over the angle and the

position z, the probability to scatter N times is then

$$P_{\mathrm{N}} = \frac{1}{1 - cos(\theta_{\max})} \int_{\theta=0}^{\theta_{\max}} \sin(\theta) \int_{0}^{1} P_{inel,N}(z,\theta)\ \mathrm{d}\theta. \tag{2.12}$$

The total response function can be retrieved from the transmission function and the functions describing the energy loss. It is given by

$$R(qU,E) = \int_{0}^{E-qU} T(qU, E\ -\ \epsilon) \sum_{i=0}^{\infty} P_N \cdot f_N(\epsilon)\mathrm{d}\epsilon. \tag{2.13}$$

2.3.3 Integral β-spectrum

Combining the differential decay spectrum with the response function, whose main contributions are the transmission function, the energy loss function and the scattering probability function, leads to the integral β-spectrum

$$I(qU) = N \cdot \int_{qU}^{E_0} \frac{\mathrm{d}\Gamma}{\mathrm{d}E}(E) \cdot R(qU,E)\,\mathrm{d}E + B \tag{2.14}$$

with N being a normalization factor and B a background rate of the experiment.

Chapter 3

Column density monitoring devices

One of the strengths of the KATRIN experiment is its ability to achieve a high source activity. Producing and detecting a high number of β-decay electrons is vital to reduce the statistical uncertainty in the neutrino mass measurement. With the ambitious goal of improving the sensitivity on the neutrino mass by one order of magnitude not only statistical but also systematic uncertainties have to be drastically reduced. It is therefore required to monitor the column density of the tritium source with high accuracy.

In this chapter the main experimental parts of KATRIN that can monitor the column density are described. At first, section 3.1 addresses the necessity of monitoring the column density. It is followed by the description of the monitoring devices. Starting in the rear section of the experiment, first the monitoring with the electron gun is outlined in section 3.2. It is followed by the description of the BIXS detector, which is located in the rear section as well, in section 3.3. A flowmeter sensor in the tritium loop system measures the throughput of the gas and is adressed in section 3.4. Further down the beamline the Forward Beam Monitor (FBM) is able to measure the activity of the tritium source. It is described in detail in section 3.5. The chapter is concluded with section 3.6 where the monitoring of the source activity with the focal plane detector is explained.

3.1 Column density stability

The column density ρd is a major systematic effect in the KATRIN experiment. It determines the amount of gas molecules, that are inside the source. In combination with the tritium purity the column density gives the activity of the WGTS. The product of ρd with the cross section σ determines the scattering probability of the β-electons in the source.

A precise knowledge of the absolute value and the variation over time is crucial for the KATRIN analysis. The absolute value has to be known to determine the scattering probabilities of the electrons with great precision. Since the KATRIN experiment measures an integral β-spectrum, variations of the column density during a tritium scan can bias the analysis of the tritium data. To mitigate these effects the KATRIN experiment features different monitoring devices, that can measure the absolute value of the column density as well as observe fluctuations on small time scales.

3.2 Photo-electron source

One of the tasks of the photo-electron source, a calibration device that was developed to provide a mono-energetic and angular-selective electron beam, is to determine the column density with a precision of 0.2 % [AAB+05].

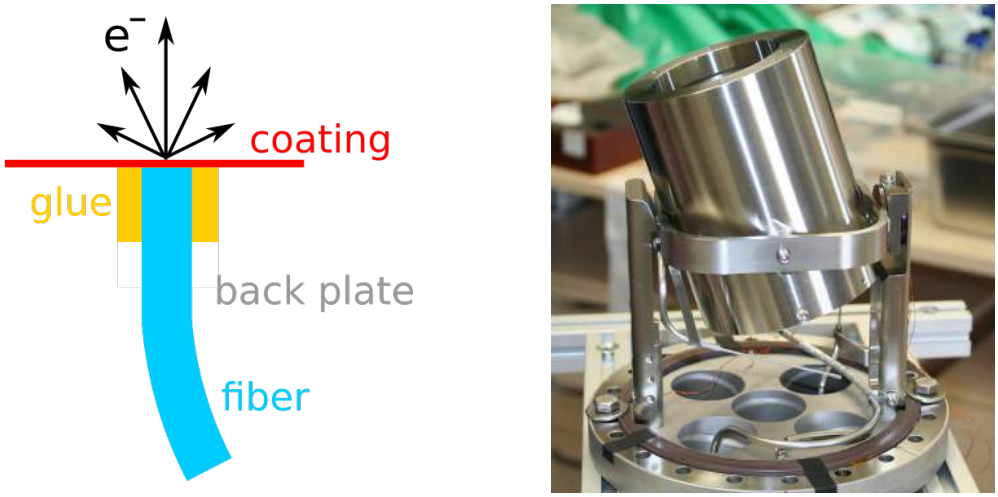

Figure 3.1: Illustration of the production of electrons with the photoelectric effect (left). A fiber guides UV light towards a photocathode, which consists of a thin metallic coating. Illuminated from behind the metal surface emits electrons with defined energy.
The setup of the electron gun (right). The grounded cage contains the acceleration setup, which is described in figure fig. 3.2, and is installed in a gimbal mount allowing the movement around two axes. A vacuum flange sealing the device in the rear section contains the feed-throughs needed for the optical fibers, HV and movement control. Taken from [Zac14] and [Beh16].

Situated in the rear section of the experiment, it emits electrons from a metal surface via the photoelectric effect as depicted in figure fig. 3.1 (left). The experimental setup is given in figure fig. 3.1 (right). Photons, produced by a light source, with a well defined wavelength are guided to a photocathode using optical fibers. There they create electrons with an energy E depending on the photon frequency and the work function of the cathode:

$$E = h\nu - \Phi > 0. \tag{3.1}$$

To reach their nominal energy E_0, which is set to be close to the tritium endpoint the electrons are accelerated against the ground electrodes at the spectrometer entrance.

Electrons that are emitted from a flat photocathode exhibit angles that follow a $\cos\theta$-distribution [PB02]. By applying a non-adiabatic acceleration electrons with a well-defined angle can be produced. For this, the electron source features a setup as depicted in figure fig. 3.2. The potential difference between the back plate and the front plate $U_{\text{acc}} = U_{\text{front}} - U_{\text{back}}$ creates a strong homogeneous electric field. Tilting the whole setup by a defined angle with respect to the magnetic field lines causes a strong non-adiabatic acceleration of the electrons narrowing their the angular distribution. This technique allows the calibration of a variety of experimental properties, for which distinct angular settings are needed [Beh16; Zac14].

To produce the electron beam the e-gun can be operated using two different light sources: a pulsed laser that produces monochromatic UV light with a wavelength of 266 nm, and a laser-driven light source (LDLS), which can create photons with a variable wavelength from about 240 nm to 320 nm. To monitor the light intensity a beam splitter in combination with a photodiode is used.

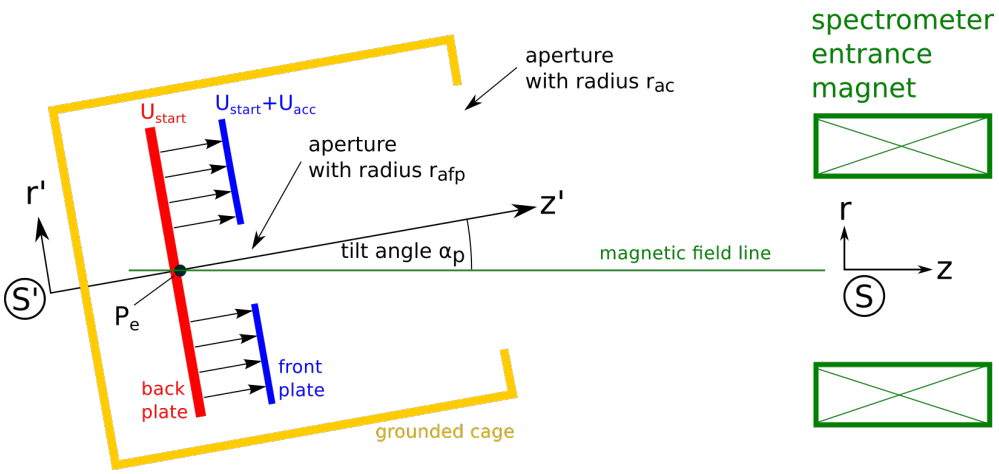

Figure 3.2: Schematic overview of the electron source setup. Created via the photo-effect from a photocathode on the back plate the electrons are accelerated in a strong electric field created by the potential difference between front plate and back plate. The grounded cage, that is shielding the potentials from outside influences, can be rotated around P_e resulting in a tilt angle α_P against the direction of the magnetic field. Figure taken from [Zac14].

For the determination of the column density with the electron gun the electrons are sent through the WGTS towards the focal plane detector and the count rate is measured at different surplus energies $\delta E = E - qU$. The obtained data is fitted to a model response function and the absolute value of the column density can be extracted as a result of the fit with high precision. This method was implemented in the frame of this thesis and is explained in more detail in chapter chapter 4.

Since this determination of ρd with the e-gun can not be conducted at the same time as the measurement of the tritium spectrum it should be applied in order to maximize the time available for the measurement of the neutrino signal. In this work a study with Monte Carlo (MC) data to reduce the time needed for a precise determination of the column density with the electron gun is given in chapter chapter 6.

3.3 Beta Induced X-ray Spectrometry

The activity of the WGTS can be monitored with the technique of the Beta Induced X-ray Spectrometry (BIXS) [MWH98]. The underlying principle is the detection of bremsstrahlung X-rays, that are produced by the β-electrons from the tritium decay. The intensity of the measured photons can be translated into the tritium activity of the WGTS.

In KATRIN two BIXS detectors are located in the rear section of the experiment as shown in fig. 3.3. They are positioned in a way to monitor the intensity of X-rays created at the rear wall surface. Almost all of the β-electrons reach the rear wall either directly or by being reflected back due to the filtering principle of the pre- and main spectrometer. This high flux of β-electrons creates intense X-Ray radiation which can be monitored by the BIXS detectors. To shield the silicon drift detectors (SDD), which detect the photon signals, from the tritium gas of the WGTS, two transparent gold-coated beryllium windows are positioned

in front of the them. The coating of the windows with gold helps to reduce the detection of X-rays which are not produced at the rear wall but are created by absorbed tritium.

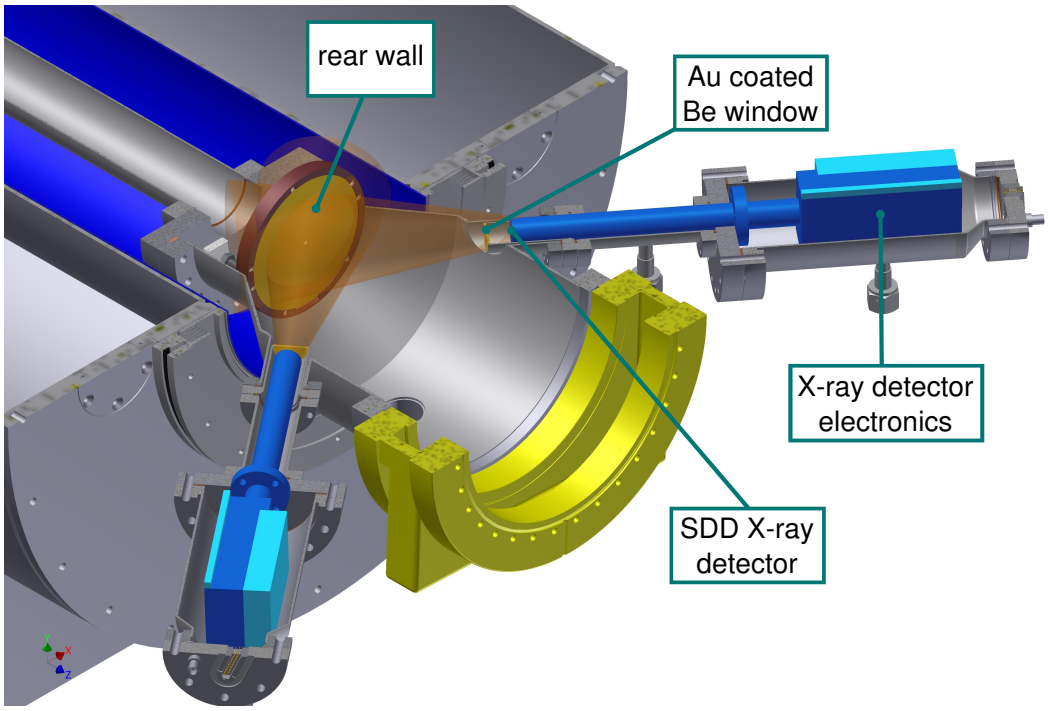

Figure 3.3: Overview of the main BIXS related experimental components. Electrons created via β-decay in the WGTS reach the rear wall and produce X-rays. These photons are detected by two silicon drift detectors, which are protected from tritium contamination by transparent gold-coated beryllium windows. Adapted from [Röl15].

To monitor the column density of the tritium source with the BIXS detectors in addition to the precise determination of the activity also the tritium purity has to be known accurately. The amount of produced X-ray radiation relates to the active part of the source gas. To monitor the absolute amount of gas molecules in the WGTS the measured activity has to be corrected with the value of the tritium purity which is measured separately via laser Raman spectroscopy (LARA). Further it is important to mitigate contaminations of the rear wall and beryllium window surface, since these would affect the amount of X-rays detected and therefore influence the measurement of the activity.

Using the BIXS detectors an accurate monitoring of the relative change of the column density is possible. Due to the observation of an intense X-ray signal the fluctuation of the activity can be determined with high precision on a short timescale. However, a precise measurement of the absolute value of ρd is not possible and is also not the intention of the Beta Induced X-ray Spectrometry [Röl15].

3.4 Tritium loop sensor

As explained in section 2.2.1, the tritium gas of the WGTS is circling in a closed loop system to create a stable column density in the source. A variety of dedicated sensors is measuring

constantly parameters like the pressure, temperature and gas flow in this complex system. By observing the relative change of the values of these parameters the column density can be monitored accurately.

One sensor that is located close to the inlet of the tritium gas into the WGTS measures the flow of the gas through the pipe $\frac{\mathrm{d}V}{\mathrm{d}t}$. Combining it with the value for the buffer vessel pressure P_{buffer} allows the determination of the throughput q:

$$q = \frac{\mathrm{d}V}{\mathrm{d}t} \cdot P_{\mathrm{buffer}} \tag{3.2}$$

The column density of the tritium source can then be estimated using gas flow simulations based on the throughput value input. This allows the determination of the absolute value of ρd with a precision of $\approx 2\,\%$ [Kuc16]. In Addition the observation of the throughput with the flow meter allows the monitoring of the column density stability during tritium measurements with good accuracy.

3.5 Forward Beam Monitor

Similar to the BIXS detector the Forward Beam Monitor (FBM) can measure the activity of the tritium source. It is situated at the end of the transport section, shortly before the β-electrons enter the pre-spectrometer. With the experimental setup, as shown in fig. 3.4, it can be inserted directly into the flux tube of the beamline. Being movable radially as well as linear in the x-direction it can be positioned over the whole flux tube area. The silicon *p-i-n* diodes have an energy resolution of $\sigma_{\mathrm{FWHM}} \approx 2\,\mathrm{keV}$.

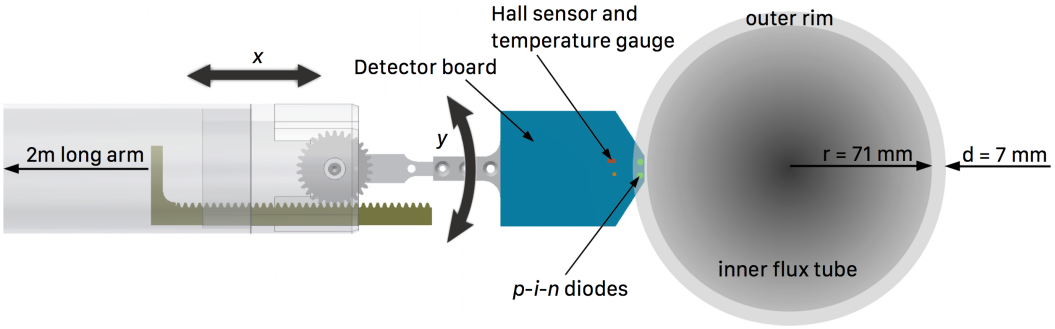

Figure 3.4: Schematic overview of the experimental setup of the FBM. The silicon detector consisting of two *p-i-n* diodes is sitting on a detector board, that is in addition equipped with a hall sensor and a temperature gauge. A 2 m long bellow enables the positioning in the flux tube. The standard monitoring position is at the outer rim of the flux tube [Are+18].

During tritium decay measurements the FBM can monitor the β-electron flux with high precision due to the large number of electrons being detected. To maximize the statistics the energy threshold can be lowered to allow also the detection of low energetic electrons. In addition to the count rate, the FBM also measures the β-spectra, allowing further study of these data.

To monitor the column density the activity, that the FBM measures, has to be corrected by the tritium purity. It is then possible to precisely determine relative fluctuations of ρd.

The absolute measurement with high precision is similar to the case of the BIXS detector not feasible.

3.6 Focal Plane Detector

The activity of the tritium source is also imprinted in the β-spectrum that is measured with the FPD. Measurement points deep in the spectrum provide a strong signal that is sensitive to activity fluctuations of the WGTS.

To accurately monitor the column density with this method corrections have to be applied to the measured electron rate. One of these corrections arises due to the uncertainty of the high voltage setting. When comparing the electron rates at a certain retarding potential, deviations in the rate can arise due to slightly different voltage settings. The measured electron rate therefore has to be adjusted to the underlying voltage value. Since the FPD measures the electrons that traverse both spectrometers the ability to overcome the retarding potentials depends on the energy loss in the WGTS. For higher column densities, assuming the tritium purity stays constant, the activity in the source is larger resulting in a higher electron rate measured at the FPD. At the same time the probability to undergo inelastic scattering in the source is increased reducing the chance of electrons to overcome the retarding potential. Hence, a correction is applied that counters this effect. As in the other activity measurements the data has to be corrected by the tritium purity to be sensitive to the whole amount of gas in the WGTS.

By monitoring the electron rate that is measured deep in the β-spectrum and applying the necessary corrections one is able to determine column density fluctuations with the FPD. The uncertainty of this measurement depends on the total number of detected electrons as well as the uncertainties of the underlying corrections. In addition spending time at a measurement point far away from the expected neutrino signal reduces the available time for the neutrino mass measurement. Fluctuations of the column density can therefore be observed only on the time scale of hours.

Another possibility to obtain the column density, which was investigated in this thesis, is from the tritium spectrum itself. Here the column density is treated as a free parameter in the spectral fit. More details are given in section 7.1.

Chapter 4

Determination of ρdσ with the photo-electron source

The goal to measure the neutrino mass with a sensitivity of 200 meV with the KATRIN experiment requires a precise knowledge of the response function of the experiment. This function describes the propagation of the β-electrons from the source to the detector. An important component of the response function is the description of the energy loss of the electrons due to inelastic scattering on the gas molecules in the source. The probability for an electron to scatter in this way depends on the column density of the source ρd and the inelastic scattering cross section of the electrons σ_{inel}. Hence, a precise knowledge of ρdσ is necessary to obtain an accurate description of the response function and therefore limit the systematic uncertainty of the neutrino mass measurement. To achieve the goal of the KATRIN experiment to measure the neutrino mass with a sensitivity of 200 meV requires ρdσ to be known with a precision of 0.2 % [AAB+05].

A determination of the column density and the inelastic cross section can be achieved with dedicated measurements using the photo-electron source. A mono-energetic electron beam with a high and stable rate is created in the rear section of the experiment and guided through the beamline towards the detector. Traversing the source, the electrons can undergo inelastic scattering and in the process lose energy. Only the electrons, that still have enough energy to pass the spectrometers are observed at the detector. Measuring the electron rate at different retarding potentials and fitting the model of the response function with ρdσ as a free parameter to this data allows an accurate determination of ρdσ.

This chapter describes in detail the necessary components to retrieve the column density and the inelastic scattering cross section from a measurement with the electron gun. It is structured in the following way: Section 4.1 describes the response model of the electrons created with the e-gun. The measurement principle to determine the column density with these photo-electrons is addressed in section 4.2. A brief overview of the software framework, that is used in the analysis, is given in section 4.3. The chapter is concluded with section 4.4, in which the determination of ρdσ with a response fit is explained and the results of the ρdσ determination for the first neutrino mass measurement are shown.

4.1 Response model

The electrons created with the e-gun differ from the β-electrons of the tritium decay in regard to the starting position, the energy and the angular distribution. Since they are used in a variety of calibration measurements, that cover different parts of the experimental setup, they are produced at a fixed position in the rear section of the experiment, as explained in section 2.2.1. A narrow energy distribution of the electrons as well as the ability to

produce them with a specific pitch angle θ is mainly required to investigate the transmission properties of the spectrometer. A precise description of the response function for the photo-electrons is necessary to infer the column density from the measured data. It has to include the properties of the e-gun electrons, that differ from the properties of the β-electrons, whose model was described in section 2.3.

4.1.1 Transmission function

The electrons created in the electron gun start in the rear section of the experiment and are guided magnetically towards the detector. Similar to the β-electrons they can only surpass the main spectrometer, if they possess more energy in the longitudinal direction than is required to overcome the retarding potential.

In the case of an ideal electron source, that produces mono-energetic electrons with pitch angles of 0°, the transmission function can be described as a step function. All the electrons with a positive surplus energy $E - qU$ in the analyzing plane are able to traverse the spectrometer and can travel towards the FPD.

The actual photo-electron source of the KATRIN experiment produces electrons with a narrow energy and angular distribution and can be adjusted to emit electrons with a certain pitch angle θ. The transmission function has to take these properties into account and can be described by

$$T(E, qU) = \int_{E-qU}^{\infty} \eta(E_e) \int_{0}^{\theta_{\max}} \xi(\theta)\, \mathrm{d}\theta \mathrm{d}E_e. \tag{4.1}$$

Including the integration over the energy and the angular distribution the function now accurately describes transmission of the electrons [Beh16].

4.1.2 Energy distribution

The e-gun uses the photoelectric effect to create the electrons by illumination with UV light with a frequency ν onto a metal surface. The energy of the created electrons is hence

$$E = h\nu - \Phi > 0, \tag{4.2}$$

where Φ is the work function of the metal surface. Because the electrons, that are situated in the metal, exhibit an energy distribution according to the properties of the photocathode material, the frequency of the illuminating light can be used to narrow the energy distribution of the emitted electrons, by tuning it to match the work function.

A simple theoretical expression of the emission of electrons via the photoelectric effect was given more than 50 years ago by Berglund and Spicer [BS64a; BS64b] and is based upon the work of Fowler, who studied the dependency of the photoelectric current on metal temperatures [Fow31]. The simplified model explains the photoemission in three steps: the excitation of the electron in the photocathode material, the transportation towards the surface and the emission into the vacuum. Starting at the beginning of the three step process and assuming a metallic photocathode, the electron resides in the conduction band and is excited by a photon with a frequency in the ultraviolet region. The energy of the excited electron depends on the photon energy as well as on the band structure of the cathode material. On the way towards the surface the electron has a large probability to scatter with

the bulk and surface material and therefore alter its initial direction and energy. Arriving at the surface the electron can be emitted into the surrounding vacuum if its kinetic energy in the normal direction is large enough to exceed the work function of the photocathode. A more detailed description of this three step model can be found in [Beh16; GB76].

The energy distribution following the theoretical model by Berglund and Spicer can be described with a generalized normal distribution of the second kind [HW97], which is an asymmetric Gaussian function and shown in eq. (4.3). The physical reason behind this non-symmetric shape is the contribution of the band structure, which features a higher number of low energetic states, to the energy distribution of the emitted electrons. The asymmetry is addressed with the shape factor κ, that returns a symmetric Gaussian when approaching zero. The mean energy of the electrons is given by $\hat{E}$ and the width of the distribution by σ_E.

$$\eta(E) = \frac{1}{\sqrt{2\pi}} \cdot \begin{cases} \frac{1}{\sigma_E} \cdot \exp\left(-\frac{1}{2}\left[\frac{E-\hat{E}}{\sigma_E}\right]^2\right) & (\kappa = 0) \\ \frac{1}{\sigma_E - \kappa(E-\hat{E})} \cdot \exp\left(-\frac{1}{2\kappa^2} \cdot \ln\left[1 - \kappa\frac{E-\hat{E}}{\sigma_E}\right]^2\right) & (\kappa \neq 0) \end{cases} \tag{4.3}$$

An energy distribution with a realistic width of 150 meV and a shape factor of 0.1 is shown in fig. 4.1. Due to the fact that only electrons with a positve energy can leave the surface of the photocathode the distribution is cut off at $E = 0$ [Beh16].

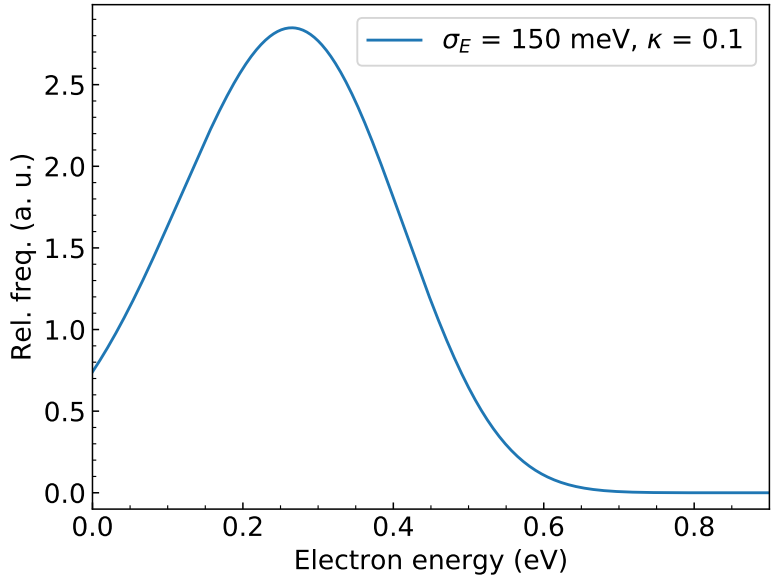

Figure 4.1: Energy spectrum of the e-gun described with a generalized normal distribution. The asymmetric distribution characterized by the shape parameter κ features only positive energy values. The depicted energy distribution has a realistic energy width of 150 meV and a shape factor of 0.1 to describe the excess of low energetic electrons due to the energetic dependency on the band structure of the cathode material.

4.1.3 Angular distribution

The electrons that are emitted from the photocathode exhibit an isotropic angle distribution. To produce a beam with only a narrow angular spread a non-adiabatic acceleration is applied to the photo-electrons. This can be achieved with a strong electrostatic acceleration, that acts on the still low energetic electrons in the presence of the guiding magnetic field. The experimental setup that is necessary for this technique was described in section 3.2. The angular distribution that is created in this way can be assumed to be Gaussian and features an angular spread of typically less than 5°. By tilting the electron source by a specific plate angle α_p, distributions with pitch angles ranging from 0° to 90° can be produced.

If the angular distribution is described by the pitch angle θ, that can take values from 0° to 90°, one has to take into account, that for small pitch angles a part of the distribution lies in the region of negative values. To take this effect into account, the distribution in the negative regime can be converted into positive values by describing the distribution with the sum of two Gaussian functions. They both have the same mean angle $\hat{\theta}$ and width σ_θ and are placed around the axis, that corresponds to a pitch angle of 0°, in a way, that one of the Gaussians is mirrored with respect to the axis. The function, that is then valid for pitch angles ranging from 0° to 90°, is given in equation eq. (4.4). The conversion of the negative distribution into the positive region is strongest in the case of θ approaching small values. For large pitch angles this function corresponds to a simple Gaussian.

$$\xi(\theta) = \frac{1}{\sqrt{2\pi\sigma}} \cdot \left[\exp\left(-\frac{(\theta - \hat{\theta})^2}{2\sigma_\theta^2} \right) + \exp\left(-\frac{(\theta + \hat{\theta})^2}{2\sigma_\theta^2} \right) \right] \tag{4.4}$$

Figure 4.2 shows an angular distribution described in this way for realistic values of an electron beam that was adjusted to have a small pitch angle. The measurement of the column density with the electron gun is also performed with electrons that feature a pitch angle which is close to 0°.

The description of the angular distribution, that was shown above, as well as the energy distribution, that was addressed in section 4.1.2, can be included into the transmission function of the photo-electrons. Integrating over the energy and the pitch angle, as explained in section 4.1.1, the description of the transmission now includes the electron properties accurately.

4.1.4 Response function

The response function includes in addition to the transmission property of the photo-electrons the energy loss, that is possible when these electrons traverse the source of the experiment. Because the e-gun electrons are created in the rear section of the experiment, they can be described to originate at the same position on the z-axis. In addition to the position, the scattering with the molecules of the source gas also depends on the inelastic scattering cross section σ_{inel}, as explained in section 2.3.2. This cross section is energy dependent and therefore has to be calculated according to the energy of the photo-electrons. Taking all this into account leads to a response function, that is given by

$$R(E, qU) = \int_0^{E-qU} T(E - \epsilon, qU) \sum_{i=0}^{\infty} P_N \cdot f_N(\epsilon) \mathrm{d}\epsilon. \tag{4.5}$$

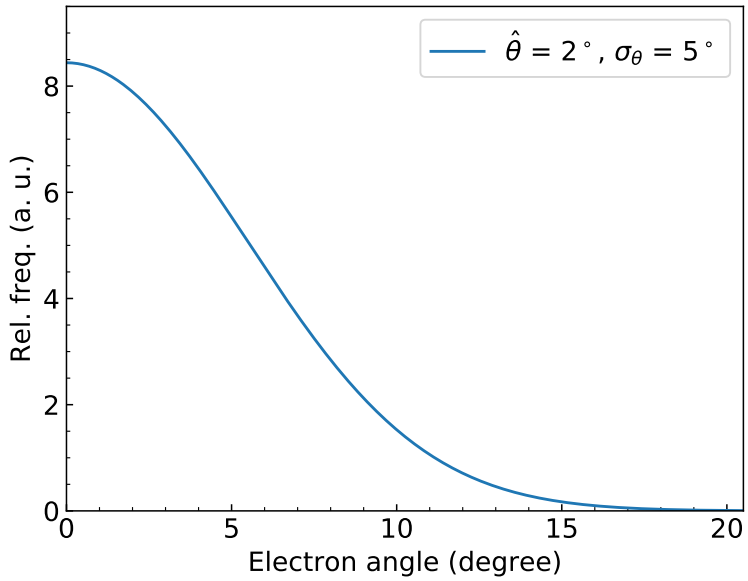

Figure 4.2: Angular distribution of the e-gun projected onto the azimuthal axis.

4.2 Measurement principle

The measurement of the column density with the electron gun consists of the observation of the electron rate for different retarding energies qU of the spectrometer. The photo-electrons produced in the rear section travel on their way towards the detector through the tritium source of the experiment, where they can scatter with the present gas molecules. In the scattering process the electrons loose energy according to the energy loss function, that was defined in section 2.3.2. The probability to undergo scattering and therefore loose energy is depending on the column density, that the electrons see along their path through the beamline. Only electrons with enough energy to surpass the retarding potential of the main spectrometer are reaccelerated and can be observed at the FPD. Hence, the rate of electrons that can be seen at the detector for different retarding energies is related to the column density. By analyzing the measured rates with a response function, that describes the propagation of the photo-electrons through the beamline, the absolute value of ρd in combination with σ_{inel} can be retrieved with high precision.

This measurement principle is illustrated in fig. 4.3. Here the electron rate is measured at three different retarding energies. The comparison with the response function, that contains the information about the column density, is indicated as well.

This goal to accurately determine ρdσ with the electron gun introduces a condition to the electron rate, that is produced at the photocathode. It has to be stable over the period of time that is needed for the measurement of ρdσ. Fluctuations in the rate of the photo-electrons can bias the result of the column density and need to be mitigated.

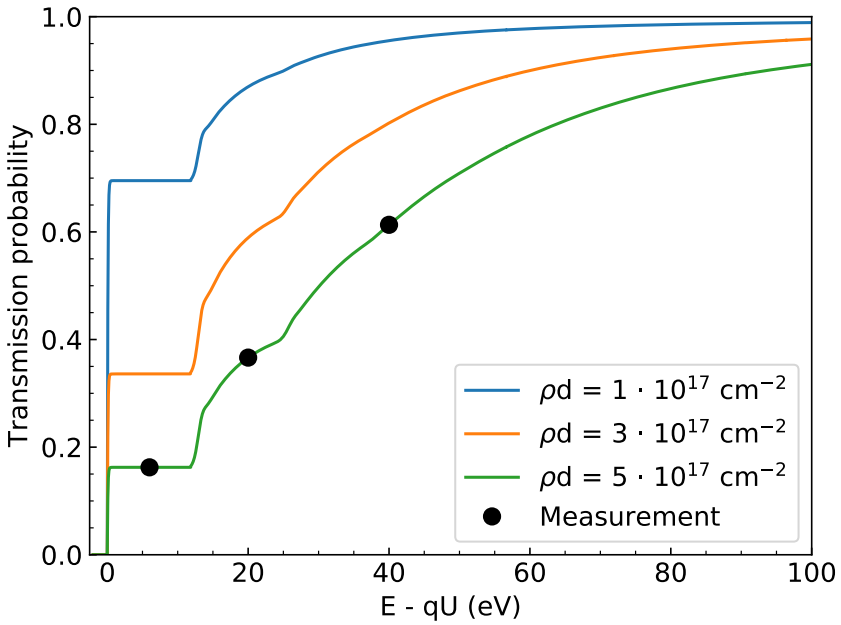

Figure 4.3: Illustration of the column density measurement with the e-gun. A response model of the photo-electrons, here shown for three different column density values, is fit to the measured electron rates at different retarding potentials. This enables the determination of the column density ρd in combination with the inelastic scattering cross section σ_{inel}.

4.3 Fitting strategy

In the course of this thesis the analysis tool Fitrium (Fit Tritium), which was developed by Christian Karl [Kar18] and Martin Slezák, is used. It includes source models for the tritium β-decay, krypton and the photo-electron source. It features a description of the KATRIN apparatus and has applications for the generation of MC data and for data fitting. In the course of this thesis the model description of the electron gun was adjusted to feature the energy and angular distribution of the electron beam, as described in section 4.1.2 and section 4.1.3.

To fit a model that is implemented in Fitrium to data, the maximum likelihood estimation is used. In this case the likelihood function can be defined as

$$\mathscr{L} = \mathscr{L}(\theta, \mu | x), \tag{4.6}$$

where it describes the probability of an experiment x, given a model μ with the parameters θ. In the likelihood estimation the model that describes the data in the most accurate way is found by estimating the parameters θ such that the likelihood function is maximized. However, for numerical reasons it is favorable to minimize $-\ln \mathscr{L}$. In the case of a model prediction with high statistics this minimization is equivalent to the χ^2-minimization:

$$-\ln \mathscr{L}(\vec{\mu}|\vec{N}) = \frac{1}{2}\chi^2(\vec{\mu}|\vec{N}) \tag{4.7}$$

In Fitrium systematic effects can be treated in multiple ways. One way is the introduction of nuisance parameters in the fit as additional free parameters. This is a simple method that allows the study of the systematic parameters from the data itself. However, the minimization of the likelihood function becomes more challenging with an increasing number of free parameters. Another method is the Monte Carlo propagation of uncertainty. Here, a value of a systematic parameter is randomly chosen from a given distribution and then used in a fit that produces a certain result. Repeating this process many times gives a distribution of the fit parameters with a certain width, that reflects their systematic uncertainty [Kar18]. A third possible treatment, that is included in Fitrium, is the Covariance Matrix approach. To address systematic effects, the χ^2-function is expanded by inserting a covariance matrix $\mathrm{V_{tot}}$:

$$\chi^2(\vec{\mu}|\vec{N}) = (\vec{\mu} - \vec{N})^T V_{\mathrm{tot}}^{-1} (\vec{\mu} - \vec{N}). \tag{4.8}$$

This matrix is calculated by generating a large number of model spectra with varying systematic parameters according to a given distribution and calculating the variance and covariance for each data point in the spectrum. The covariance matrix then encodes the uncertainty of the systematic effect and can be summed with other covariance matrices to give a total matrix, that includes systematic and statistical uncertainties:

$$V_{\mathrm{tot}} = \sum_k V_{\mathrm{sys,k}} + V_{\mathrm{stat}} \tag{4.9}$$

This approach is justified for large counting statistics where the χ^2-minimization is valid [Sch19].

4.4 Determination of ρdσ during KNM-1

In the spring of 2019 the KATRIN experiment had its first high-purity tritium campaign. In this first neutrino mass measurement (KNM-1) the determination of the column density with the e-gun played an important role. In the following the measurements of ρdσ using photo-electrons, that were taken during this campaign, are described in full detail.

4.4.1 Photo-electron measurement

In KNM-1 ten measurements with the electron gun were performed. The total electron rate that could be achieved by the e-gun was in the order of 1500 cps (counts per second). As a source for the photons, the laser-driven light source (LDLS) was used. The retarding potentials of the main spectrometer were set in a way, that the electrons possess surplus energies of 5 eV, 50 eV, 100 eV and 200 eV respectively. The electron rate was measured at these energies more than once to counteract fluctuations and trends of the photo-electron rate. The effect of increasing the measurement time at surplus energies that are most sensitive to the column density determination can be seen by looking at the statistical uncertainties of the electron rates. The more time is spent at a certain retarding potential, the more electrons are observed, reducing the statistical uncertainty of the electron rate at this measurement point. The statistical uncertainties shown in fig. 4.4 are amplified by a factor of ten for better visualization.

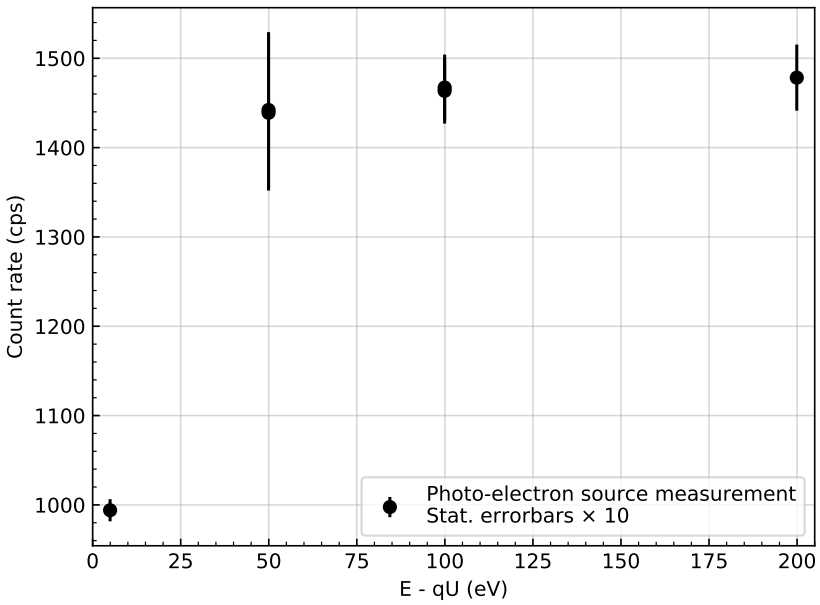

Figure 4.4: Measured photo-electron rates for different retarding energies. For better visualization the statistical errors of the electron rates are increased by a factor ten.

4.4.2 Systematic effects

To address systematic effects that can alter the result of ρdσ, that is retrieved in a measurement with the photo-electron source, the Covariance Matrix approach is used. In the following the systematic effects, that were taken into account for the column density measurement with the electron gun, are listed and briefly described:

- **HV fluctuation:** Fluctuations of the retarding potential of the main spectrometer can change the transmission probability of the photo-electrons on their way to the detector.
- **Electron energy width:** The description of the energetic distribution of the photo-electrons is a vital part of the response model and is determined with specific uncertainty.
- **B-fields:** The magnetic fields B_{S}, B_{max} and B_{ana} affect the transmission of the e-gun electrons.
- **Energy loss function:** The amount of energy that is lost in the source by scattering with the gas molecules influences the transmission probability of the photo-electrons at a certain retarding potential.
- **Detector pileup:** The electron beam covers only one of the pixels of the focal plane detector. The large electron rate causes pileup effects, that are more dominant for

higher rates. A correction can be applied to the measured data to reconstruct the true electron rate. This correction features an uncertainty that has to be addressed.

- **Non-Poisson electron rate:** The experimental setup of the photo-electron source can cause fluctuations and drifts of the electron rate. The instability of the electron rate during a column density measurement can alter the measured value of ρdσ.

All these systematic uncertainties are inserted into the χ^2-function using covariance matrices that are summed up into a total matrix V_{tot}. The relative uncertainty values, that form the basis of the matrix calculations, are listed in table 4.1.

Table 4.1: Systematic budget for a column density measurement with the electron gun.

Systematic parameter	Relative uncertainty
HV fluctuation	40 mV
Electron energy width	10 %
B_{S}, B_{max}, B_{ana}	2.5 %, 0.2 % and 1 %
Energy loss function	$\mathcal{O}$(1 %)
Detector pileup	18 % on correction term
Non-Poisson electron rate	0.25 % on electron rate

4.4.3 ρdσ fit

The column density can be determined by fitting a model response function to the measured data. Minimizing the χ^2-function, that includes the systematic uncertainties of the measurement in form of a covariance matrix, as mentioned above, and leaving the total electron rate R_{tot} as an additional free fit parameter results in the determination of the column density in combination with the inelastic scattering cross section.

The fit of an e-gun measurement of KNM1 can be seen in fig. 4.5. It shows the measured electron rates, the best fit model and the residuals. For this example measurement a value of $\rho d\sigma = 0.3981 \pm 0.0034$ could be determined. This translates into a relative uncertainty of 0.85 %, which exceeds the requirement of 0.2 % to match the KATRIN systematics budget. However, due to radiochemical reactions of the tritium gas the column density was limited during the first measurement campaign to a value, which is roughly a factor of five smaller than in the nominal setting. The signal that contains the information about the column density is more pronounced for higher values of ρdσ, leading to a more precise determination of the column density in the nominal setting. In addition the systematic uncertainties for the e-gun measurements were chosen to be conservative for this first neutrino mass campaign.

Dividing the fit result by the inelastic cross section $\sigma_{\mathrm{inel}} = 3.60 \times 10^{-18}\,\mathrm{cm}^2$ (for the photo-electron energy of 18.78 keV, adapted from [Liu87]) yields a column density value of $\rho d = 1.11 \times 10^{17}\,\mathrm{cm}^{-2}$.

The fit results of all ten measurements with the electron gun are listed in table 4.2. The corresponding fits are illustrated in fig. 4.6 and fig. 4.7.

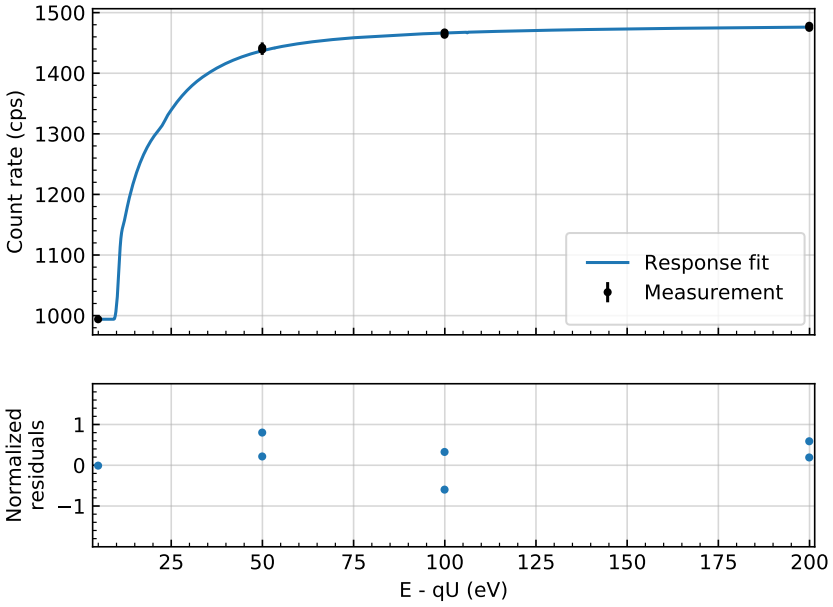

Figure 4.5: Fit of a column density measurement with a model response function. Shown are the measured electron rates, the best fit model, that was retrieved with a χ^2-minimization, and the residuals.

Table 4.2: Fit results of all column density measurements with the electron gun, that were performed during KNM-1.

Run number	ρdσ fit result	Relative uncertainty (%)
51390 + 51391	0.4060 ± 0.0020	0.49
51633 + 51634	0.3998 ± 0.0024	0.60
51635 + 51636	0.4021 ± 0.0026	0.65
51637 + 51638	0.3976 ± 0.0024	0.60
51867	0.3990 ± 0.0034	0.85
51868	0.3994 ± 0.0034	0.85
51869	0.3981 ± 0.0034	0.85
52077	0.3768 ± 0.0034	0.90
52079	0.3880 ± 0.0034	0.88
52080	0.4074 ± 0.0034	0.83

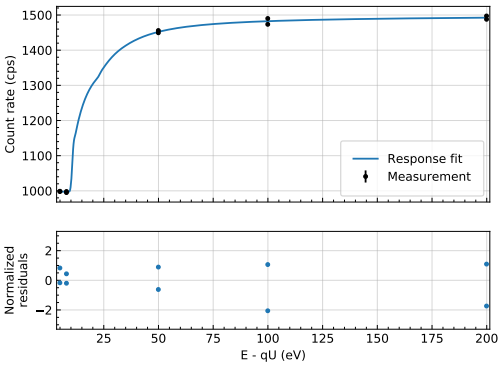

(a) 51390+51391

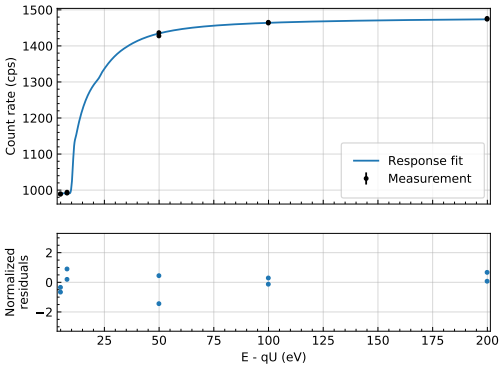

(b) 51633+51634

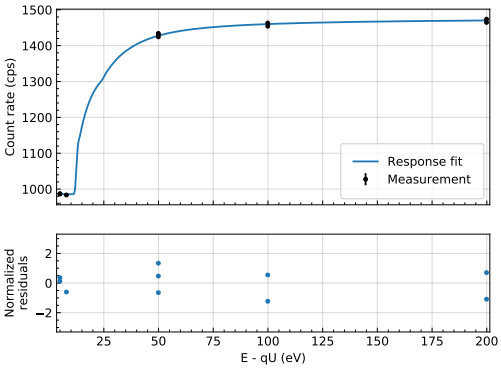

(c) 51635+51636

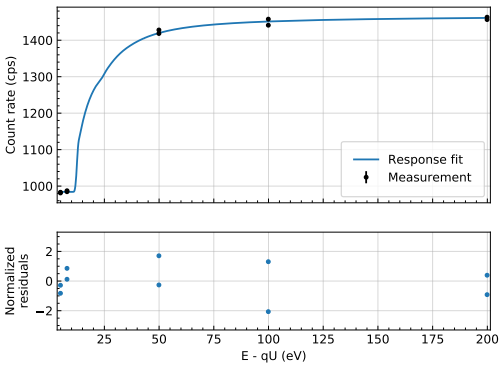

(d) 51637+51638

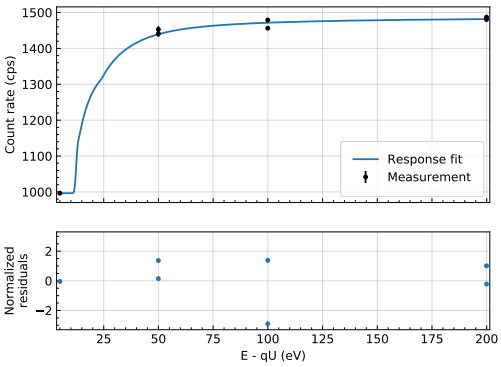

(e) 51867

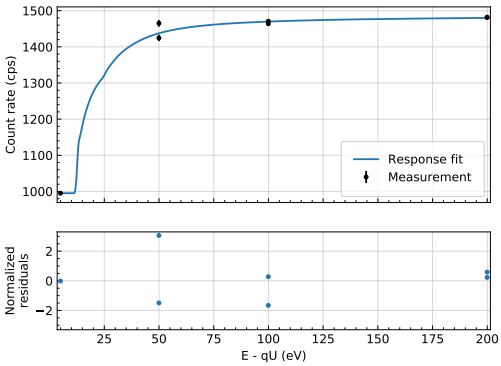

(f) 51868

Figure 4.6: KNM-1 column density measurement fits. Shown are the measured electron rates, the best fit model and the residuals.

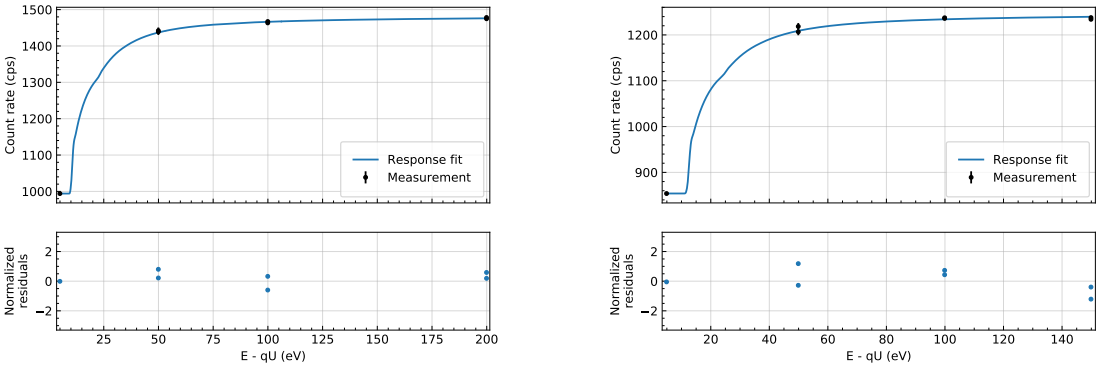

(a) 51869

(b) 52077

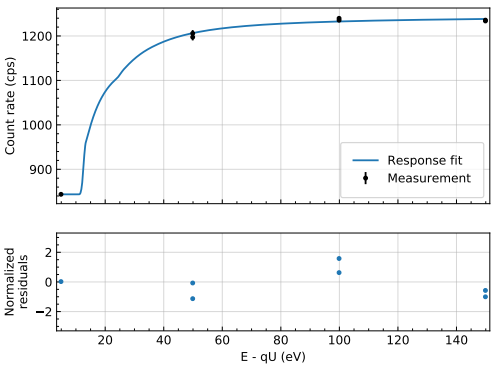

(c) 52079

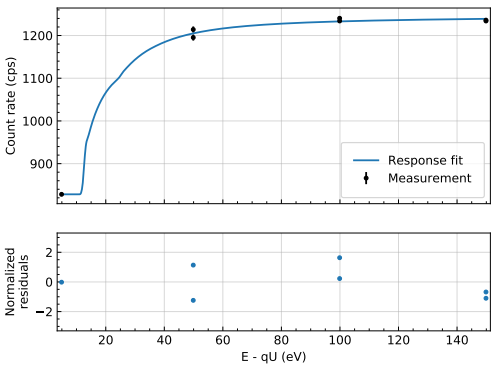

(d) 52080

Figure 4.7: KNM-1 column density measurement fits. Shown are the measured electron rates, the best fit model and the residuals.

Chapter 5

Stability of the column density during KNM-1

The KATRIN experiment had its first neutrino mass measurement in spring 2019. This first measurement campaign marks the beginning of the task to improve the sensitivity on m_ν to 200 meV (90 %C.L.) within 5 years.

In this first neutrino mass measurement the column density in the source was limited to $\rho d = 1.11 \cdot 10^{-17}$ molecules cm^{-2}. This value is approximately a factor of five smaller than $\rho d_{nominal}$. The reason for this limitation was a radiochemical reaction of the tritium gas with the steel surface of the injection capillary, that caused drifts in the column density. To contain these drifts to a level of $\pm\ 2 \cdot 10^{-2}$ during the first neutrino mass measurement, the column density was to set to this lower value.

The determination of the column density with high precision during the first measurement campaign of the KATRIN experiment was of great importance, since it is a dominant systematic effect in the neutrino mass measurement. In addition the drifts of the column density, arising from the radiochemical reactions of the tritium, had to be monitored accurately during the whole measurement period.

In this chapter the successful determination of the stability of $\rho d\sigma$ with high precision during the first neutrino mass measurement is described. This task was achieved in the course of this thesis in collaboration with Fabian Block [Blo] and Alexander Marsteller [Mar]. The chapter begins with section 5.1, that addresses the need for continuous monitoring of the column density during KNM-1 and presents a strategy to achieve this task. In section 5.2 the result of the stability of the column density is shown and its impact on the neutrino mass measurement is stated.

5.1 Continuous $\rho d\sigma$ monitoring

The radiochemical reactions of the tritium gas with the capillary surface lead to a stability of the column density on a level of $\pm\ 2 \cdot 10^{-2}$ during the first neutrino mass measurement. For this reason a precise determination of the column density for all the 274 tritium scans, that were performed during KNM-1, was not possible using only the photo-electron source measurements. A solution was found by combining the e-gun measurements with a column density monitoring device, that constantly measures the column density [Blo; Mar].

In chapter 3 an overview was given of the main experimental devices of KATRIN, that can monitor the column density. The choice of the monitoring device for the calibration with the e-gun measurements was based on the stability of the device during the measurement campaign. To determine this stability, the monitored parameter values of each device were compared to the electron rates, that were measured deep in the tritium spectrum. The β-spectrum itself can not be used for the calibration, since it is not simultaneously measured with the photo-electrons. After applying the necessary corrections to the measured rates of

the FPD, BIXS detector and FBM, as described in section 3.3, section 3.5 and section 3.6, the monitoring devices can be compared for their stability.

Figure 5.1a shows the comparison between the measured rates of the BIXS detector and of the FPD. One can see a positive correlation, that is changing over time. This implies that the measured rates at the BIXS detector are drifting over time independently of the actual variation of the activity.

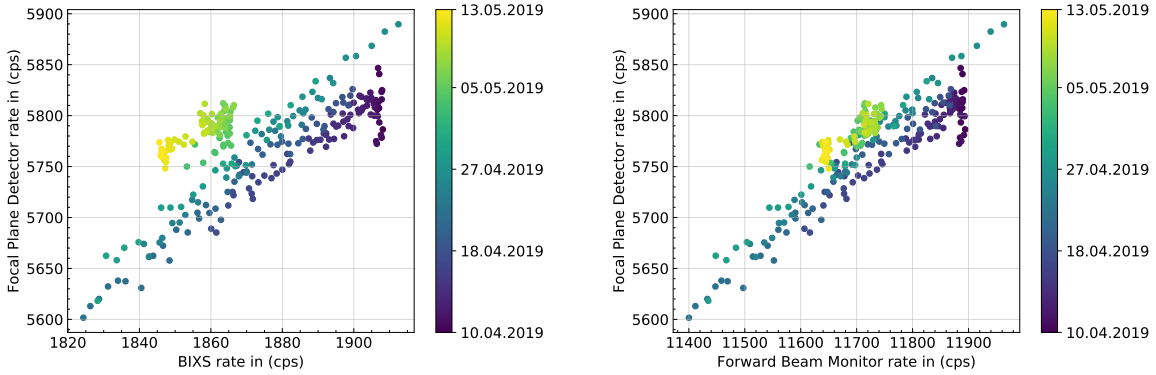

(a) Comparison of BIXS rate and FPD rate.

(b) Comparison of FBM rate and FPD rate.

Figure 5.1: The BIXS and FBM rate in comparison with the FPD rate. A timeline of the measured data is indicated in the color gradient. A positive correlation and a drift over time is visible for both monitoring devices.

The comparison of the FBM and the FPD shows a similar behavior, as can be seen in fig. 5.1b. However, the drift over time is smaller than compared to the BIXS detector.
The best correlation can be achieved when comparing the measured throughput of the flowmeter sensor with the FPD rate. This is depicted in fig. 5.2. Here, there is no significant drift over time visible.

Because the flowmeter sensor showed the best stability over the whole measurement time it was used for the calibration with the e-gun measurements. The throughput value is constantly monitored during a column density measurement with the photo-electron source. Hence, the precisely determined values of $\rho d\sigma$ can be connected to the throughput values of the flowmeter sensor. This translation is shown in fig. 5.3. The precise measurements of $\rho d\sigma$ (see section section 4.4.3) are plotted in relation to the simultaneously measured throughput values. The fit with a linear model, using the method of least squares, calibrates the throughput values to $\rho d\sigma$. The uncertainty of this calibration is given by the 1-σ confidence interval of the linear fit. The column density for each tritium scan can now be determined by translating the corresponding throughput value, that is measured during the scan, to a $\rho d\sigma$ value. The calibration script was developed in the course of the thesis of Fabian Block [Blo].

5.2 Systematic uncertainty

Using the calibration method, as explained above, allows the precise determination of the column density during the whole tritium measurement phase. The uncertainty of the deter-

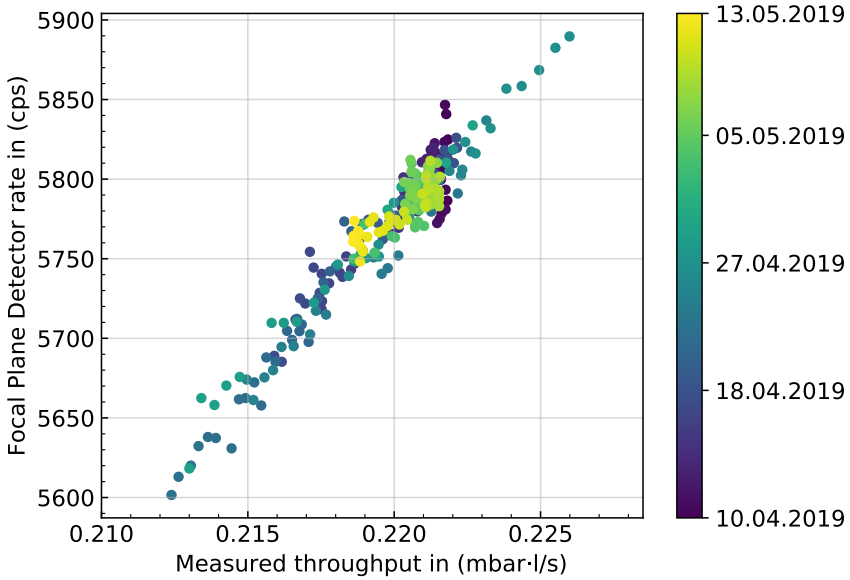

Figure 5.2: Comparison of the throughput, that is measured with the flowmeter sensor, with the rate measured deep into the β-spectrum. The colors indicate the timeline of the measurements. The flowmeter sensor shows no significant drift over time and a good correlation with the FPD rate.

mined column density value consists of three parts: The uncertainty of the translation of the throughput value to $\rho d\sigma$, the uncertainty of the flowmeter sensor and the uncertainty of the inelastic scattering cross section σ_{inel}.

The uncertainty of the translation can be extracted from the confidence interval of the linear fit. The fluctuations of the flowmeter sensor can be estimated by comparing the throughput values to the rates measured at the FPD, during a sub-measurement of the tritium spectrum at a low retarding potential [Blo]. This yields a conservatively estimated uncertainty of 0.64 % on $\rho d\sigma$ for the influence of the throughput fluctuations. The uncertainty of the inelastic scattering cross section is needed for the conversion of $\rho d\sigma_{\text{photo-electron}}$ to $\rho d\sigma_{\beta\text{-electron}}$, since the cross section is depending on the electron energy. For this conversion the error is estimated to be 0.1 % [Liu87].

Taking these three uncertainty contributions into account the column density in combination with the inelastic scattering cross section can be determined for all tritium spectrum sub-measurements with a precision of better than 0.85 %. The determined absolute values of $\rho d\sigma$ and the corresponding relative uncertainties are shown in fig. 5.4.

In the first neutrino mass measurement with the KATRIN experiment in spring 2019, the effective neutrino mass squared was found to be $m_\nu^2 = \left(-1.0^{+0.9}_{-1.1}\right)\,\text{eV}^2$. The precise determination of $\rho d\sigma$ with a relative uncertainty of 0.85 % resulted in an uncertainty for m_ν^2 of only $0.05\,\text{eV}^2$.

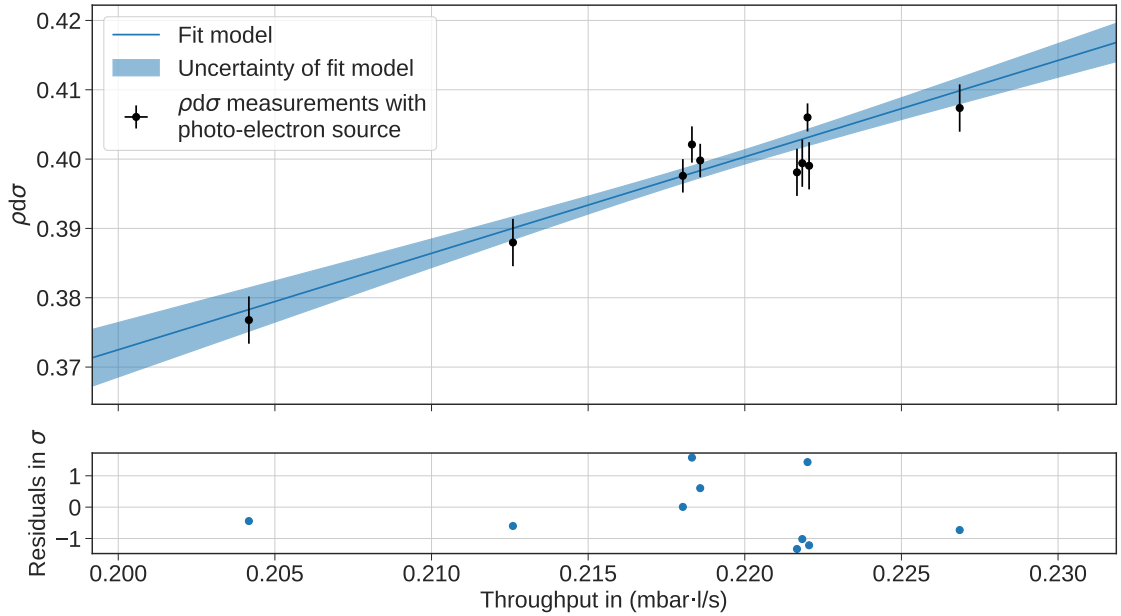

Figure 5.3: Linear translation of the ρdσ values, measured with the electron gun, to the throughput values, measured with the flowmeter sensor. The uncertainty of the translation is given by the confidence band (indicated in blue).

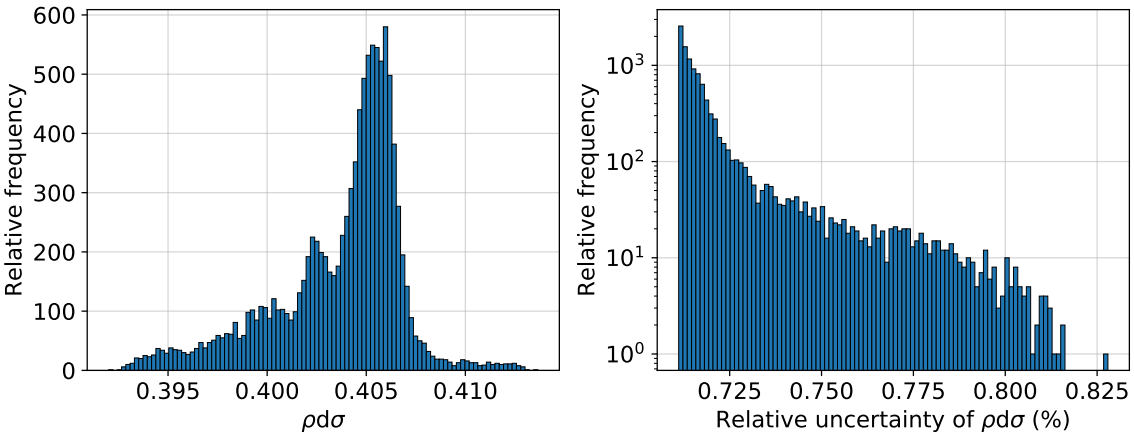

Figure 5.4: The absolute value of ρdσ for all tritium spectrum sub-measurements (left) and the relative uncertainty for the determination of ρdσ (right).

Chapter 6

ρdσ measurement time optimization

The determination of the column density with high precision can be achieved using the electron gun, as shown in chapter 4. Since a simultaneous measurement of the tritium spectrum and the e-gun beam is not possible, the time spent to retrieve ρdσ can not be used to measure the integral β-spectrum. It is therefore important to optimize the absolute time that is needed for a precise measurement of the column density using the photon-electron source.

A study aimed at this task is described in this chapter. A brief overview of the measurement of ρdσ is given in section 6.1. The optimization of the measurement time for the column density determination in the nominal KATRIN setting is addressed in section 6.2. The first neutrino mass measurement, that was performed in spring 2019, required a separate optimization, that is explained in section 6.3.

6.1 ρdσ measurement

In section 4.4.3 was shown, that fitting a response model to data measured with the photo-electron source allows the determination of the column density. The information about ρdσ is imprinted in the shape of the response model. It is favorable to set the measurement points in regions where the signal of the column density is the strongest. In addition the fraction of time that is spent at each point can be optimized. Thus the task to reduce the overall measurement time consists of finding the most suited measurement time distribution (MTD). This can be achieved by studying Monte Carlo generated data, that are produced according to a certain MTD. To reflect a realistic e-gun measurement, in addition systematic uncertainties have to be taken into account.

In the response model, that is depicted in fig. 6.1 up to 200 eV surplus energy, one can define several characteristic energy regions. For example, the plateau region, which is in the energy range of around 1 eV to 13 eV. It contains the information about the zero scattering probability of the photo-electrons. For higher surplus energies electrons can traverse the spectrometer, that have undergone inelastic scattering with the source molecules. This leads to a sharp rise in the transmission probability for electrons with energies higher than a certain value, that is determined by the energy loss function. For large surplus energies the transmission probability approaches 100 %, which would return the total rate of electrons, that is produced by the electron gun.

In order to determine the column density with the response model fit, that has two free parameters, the electron rate has to be measured with least at three different retarding energies. Setting the high voltage to a new value with high precision requires a certain amount of time before the system is stable again. These boundary conditions have to be taken into account in the search for the optimal MTD.

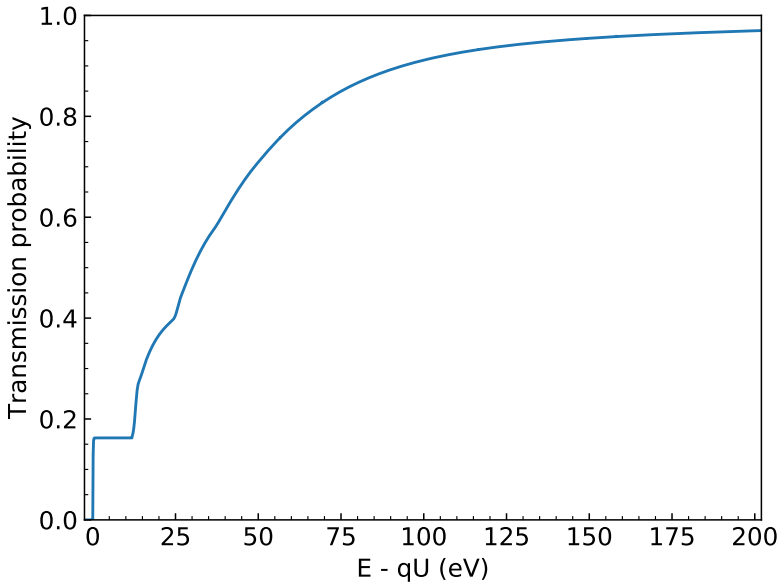

Figure 6.1: Response model for the electrons of the electron gun.

6.2 Nominal KATRIN setting

The nominal KATRIN setting features a column density of $\rho d = 5 \times 10^{-17}\,\mathrm{cm}^{-2}$. To reach the required precision in the determination of ρd of 0.2 %, it was proposed to perform the measurement according to a MTD that is shown in fig. 6.2 [AAB+05]. Here it is suggested to measure at three different retarding energies. One measurement point is situated in the plateau region, with the aim to determine the rate of electrons, which have not undergone an inelastic scattering process. The other two electron rates are measured at surplus energies of 20 eV and 40 eV, where the effect of the energy loss due to scattering is most visible. According to this MTD, the largest fraction of the time should be spent measuring at the energy region, where the electrons have undergone zero scattering. The remaining measurement time is distributed equally on the measurement points of 20 eV and 40 eV surplus energy.

In the course of this thesis a study was performed to optimize the MTD for the nominal KATRIN setting. The uncertainty of the electron was rate assumed to be 0.1 %, which is the requirement for the determination precision of $\rho d\sigma$ of 0.2 %. In addition systematic effects for the energy loss, the magnetic fields, the HV fluctuations and the energy width of the photo electrons were taken into account. The resulting optimized MTD is shown in fig. 6.3. Similar to the proposed measurement time distribution described above, a large fraction of the time has to be spent in the plateau region. Moreover, the study has shown, that it is advantageous to measure the electron rate at high surplus energies. In this energy region the measured rate of the photo-electrons is close to the total rate that is produced by the source. The lower the retarding potential of the main spectrometer is set, the closer the observed electron rate is to this initial rate. The limitation to surplus energies of around 200 eV arises due to the experimental setup of the electron gun. Measuring in this energy region is advantageous to the determination of the column density, since the total electron

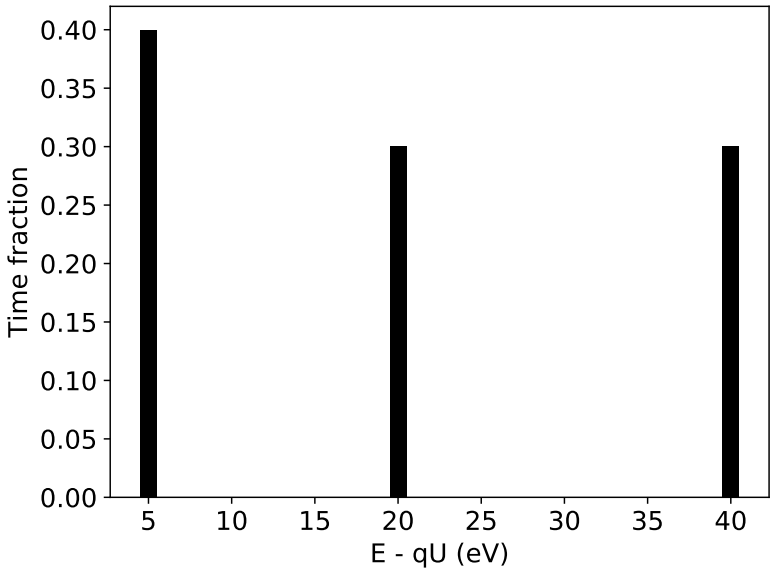

Figure 6.2: Measurement time distribution for the column density measurement in nominal KATRIN operation mode, according to [AAB+05]. The largest fraction of the time is spent on the plateau region.

rate R_{tot} is set as an additional free parameter in the fit and can therefore be constraint by the data itself. The total number of measurement points is constraint by number of free parameters in the fit and the fact that the setting of a stable HV requires additional time. An optimum was found for four measurement points, that can be equally distributed to the two measurement regions.

6.3 First neutrino mass measurement

For the first neutrino mass measurement of KATRIN, that was performed in spring 2019, deviations from the nominal setting required a separate optimization of the MTD for the column density measurement. The column density was limited in this first measurement campaign to 22 % of the nominal value, because of chemical reactions of tritium gas with the steel surface of the tritium loop system. Furthermore, the electron gun exceeded the necessary stabilization of the electron rate of 0.1 % and was estimated to be in the order of 0.25 %. In addition the electron rate showed small drifts over time.

Taking these new conditions into account resulted in an optimized MTD, that is shown in fig. 6.4. Since it was the first measurement of KATRIN with a large amount of high-purity tritium in the source, additional measurement points in the intermediate region at surplus energies of 50 eV and 100 eV were included. The largest amount of measurement time is still spent at the plateau region. The column density measurement is therefore conducted at four different retarding potentials: 5 eV, 50 eV, 100 eV and 200 eV. To counteract drifts of the e-gun rate the retarding potentials were measured more than once in a column density scan. Separating the measurements at the same retarding potentials in time, allows to mitigate

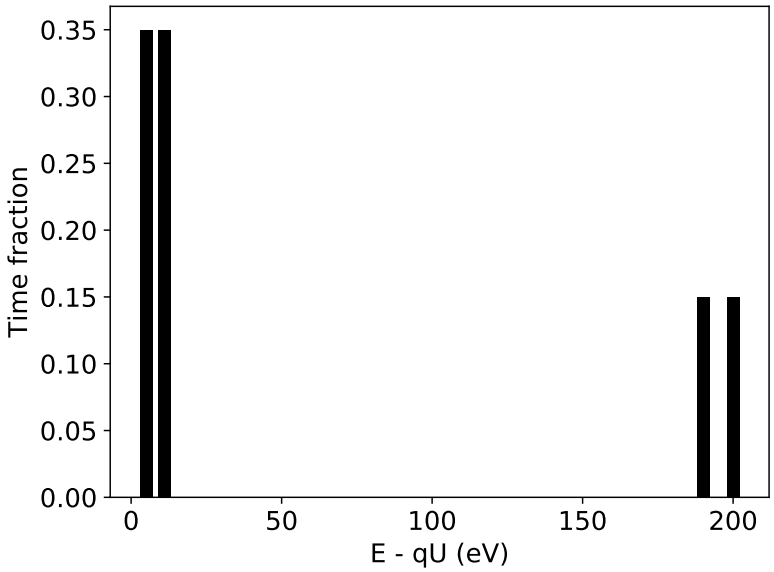

Figure 6.3: Measurement time distribution for the column density measurement in nominal KATRIN operation mode, optimized by hand. The electron rates are measured for energies at the plateau region and at high surplus energies.

the influence of the rate drifts on the column density value, that is retrieved from the fit of the e-gun data. This optimized MTD was successfully used in the determination of the column density during the first neutrino mass measurement, which is described in chapter 4.

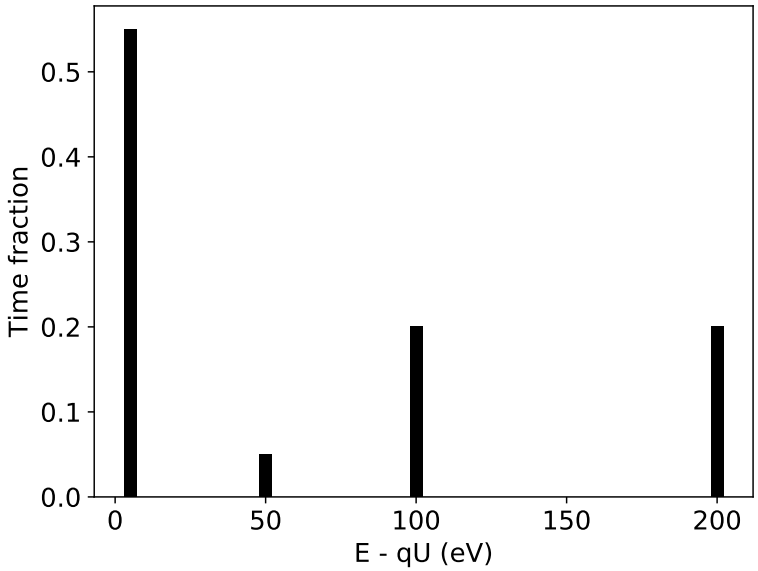

Figure 6.4: MTD for the first neutrino mass campaign. Measurement points in the intermediate region allow the validation of the response model over the whole energy range. The measurement time at 50 eV, 100 eV and 200 eV is split into two separate measurements to counteract rate drifts of the photo-electron source.

Chapter 7

Column density as an additional free fit parameter

In the standard KATRIN neutrino mass analysis there are four free fit parameters: the effective neutrino mass squared m_ν^2, the endpoint value E_0, the signal normalization A_S and the background rate R_{bg}. In addition, the column density can be set as a fifth free parameter. In this way information about the column density can be extracted from the tritium spectrum itself.

In the following chapter, section 7.1 describes the determination of ρdσ by including it as an additional parameter in the fit. Section 7.2 addresses the correlations of ρdσ to the other four fit parameters.

7.1 ρdσ determination from data

The product of the column density and the scattering cross section determines the scattering probabilities of the β-electrons in the source (see eq. (2.11)) and hence can be fitted from the measured integral β-spectrum. This strategy of determining ρdσ can be applied to the first neutrino mass measurement. For this, all measured tritium scans during KNM-1 are fitted by leaving the column density as an additional free parameter. The fit can be performed for different energy ranges of the measured tritium spectra. For large ranges the statistical uncertainty of ρdσ, determined by the fit, becomes smaller, since a higher number of β-electrons is included in the analysis.

The results of fitting the tritium spectrum with lower fit boundaries ranging from $-92.5\,\mathrm{eV}$ to $-47.5\,\mathrm{eV}$ below the endpoint E_0 are shown in fig. 7.1. In addition the average value of ρdσ, that was determined by using a combination of the e-gun and the flowmeter sensor, as explaind in chapter 5, is illustrated. The fits of the tritium spectrum include only statistical uncertainties. The comparison of the ρdσ values, that were determined by the two different methods, yields a good agreement for the fits with a large energy range. For smaller ranges there is a tendency towards lower values of ρdσ. However, in this fit range the statistical uncertainty of the determined column density value is large.

7.2 Parameter correlation

One technique to introduce systematic uncertainties into the KATRIN neutrino mass analysis is the Monte Carlo Propagation of uncertainties. Here, a fit is performed many times while the systematic input parameters are randomly chosen from a given distribution for each fit. The resulting distributions of the fit parameters provide information about the systematic uncertainty of these parameters. In addition the correlations between the fit parameters can

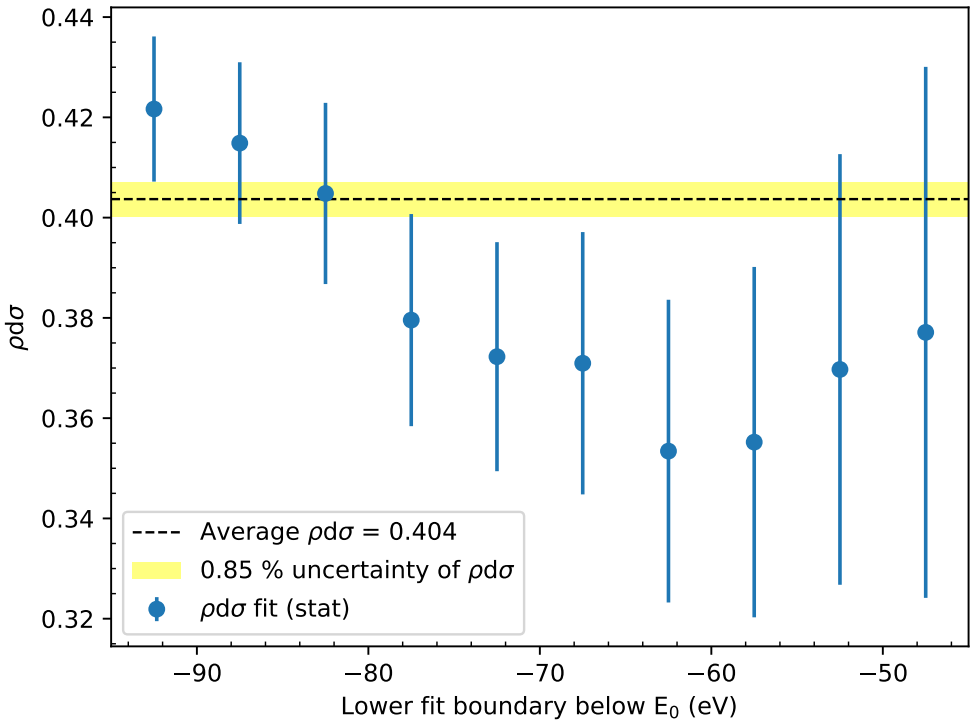

Figure 7.1: Column density fit of all the tritium scans of the first neutrino mass measurement for different fitting ranges. The average value of the column density for all the scans is indicated by the dashed, black line. It was determined as described in chapter 5. The uncertainty of the average column density is given by the yellow error band.

be studied. To include statistical uncertainties at the same time, the fits can be performed on MC generated data, that are statistically fluctuated copies of the real data set. This technique, together with the covariance method (explained in section 4.3), was used in the first neutrino mass analysis of the KATRIN experiment [AAA+19].

To study the correlations of the column density with the four standard fit parameter, the MC propagation can be extended to include ρdσ as an additional fit parameter. For this task the same fitting range and systematic input parameters were used, as in KNM-1 [AAA+19]. In total 10^4 fits were performed. A scatter plot of fit values of ρdσ and the neutrino mass squared m_ν^2 is shown in fig. 7.2. For better visualization both axes display the relative deviation of the column density and the squared neutrino mass from their best fit value, respectively. The best fit value is indicated as the point, where the two dashed lines, that represent the maximum values of the two distributions, cross. The two fit parameters have a positive correlation, that can be clearly seen by looking at the error contours of the best fit point. This can be explained by the influence of the column density on the integral β-spectrum. For an undetected shift of the column density to higher values, less high energetic β-electrons would be able to pass the spectrometer, since their probability to scatter and

loose energy in the source is higher. This would alter the shape of the integral β-spectrum near the endpoint and could be interpreted as a larger neutrino mass. For a negative column density shift the imprint on the spectrum would be in the opposite direction. The uncertainty of the ρdσ determination in KNM-1 is illustrated by the yellow error band. This relative uncertainty of 0.85 % has a minor impact on the squared neutrino mass.

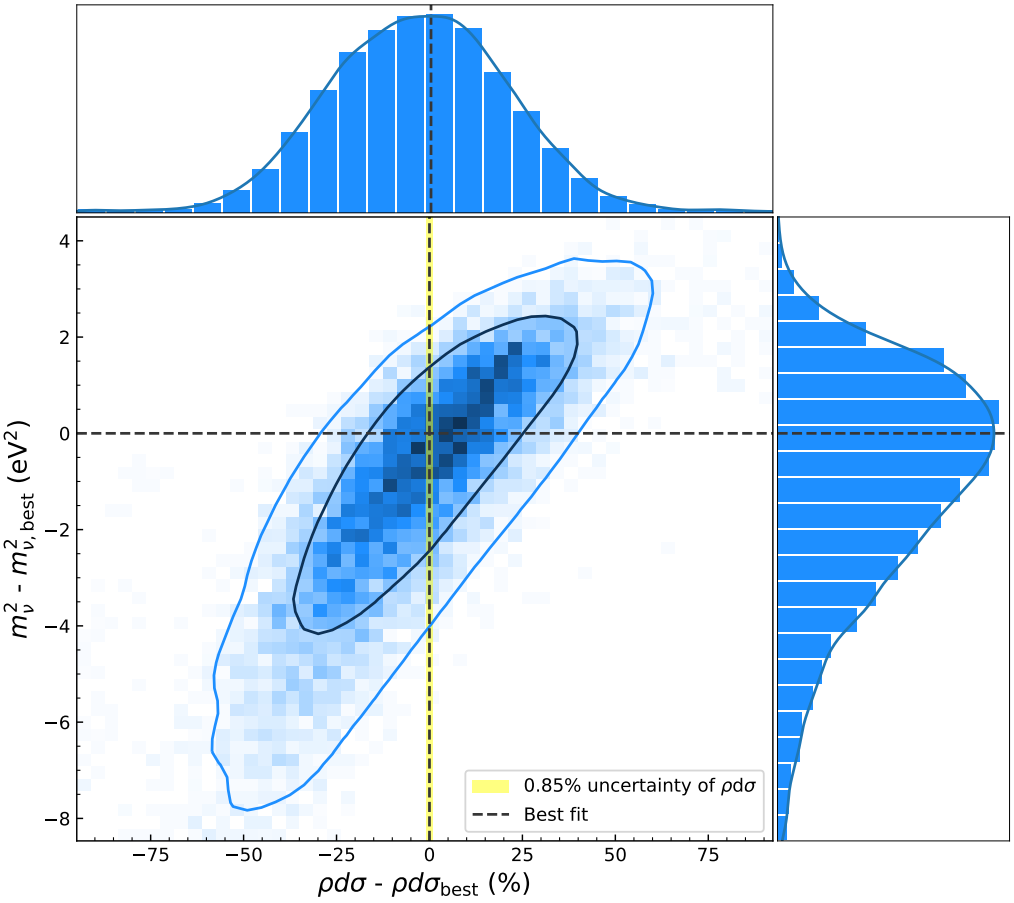

Figure 7.2: Scatter plot of fit values for the neutrino mass squared m_ν^2 and the product of column density and cross section ρdσ. The best fit value is illustrated by the crossing point of the two dashed lines. The 1-σ (black line) and 2-σ (blue line) error contours for the best fit point are outlined. The uncertainty of the column density determination in KNM-1 is indicated by the yellow error band.

The correlation with the other three fit parameters is depicted in fig. 7.3. Because the endpoint is highly correlated with the squared neutrino mass, it shows a positive correlation with the column density as well, as shown in fig. 7.3a. The activity of the source, that influences the signal normalization, is depending on the column density and the tritium purity. Increasing the column density, while still being below the maximal value, increases also the tritium activity. Hence, the signal normalization and ρdσ are positively correlated, as can be seen in fig. 7.3b. Since the tritium flow from the source to the spectrometer is reduce by 14 orders of magnitude, there should be no correlation between the background

rate and the column density, which is visualized in fig. 7.3c.

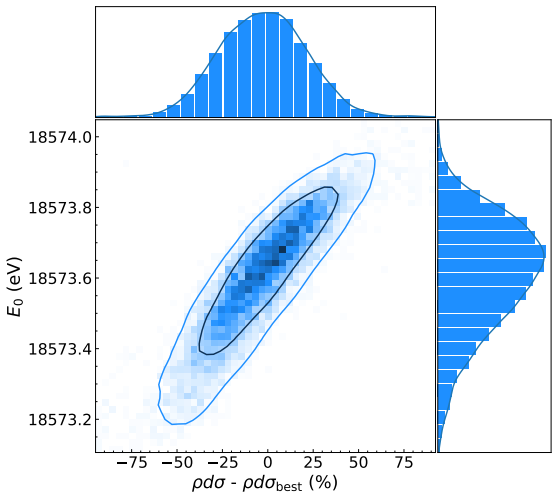

(a) Endpoint E_0

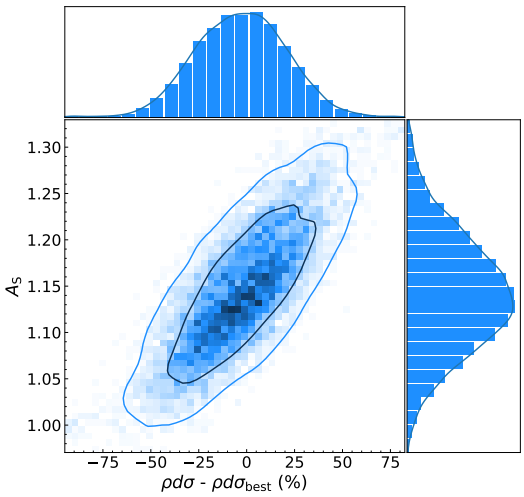

(b) Normalization A_S

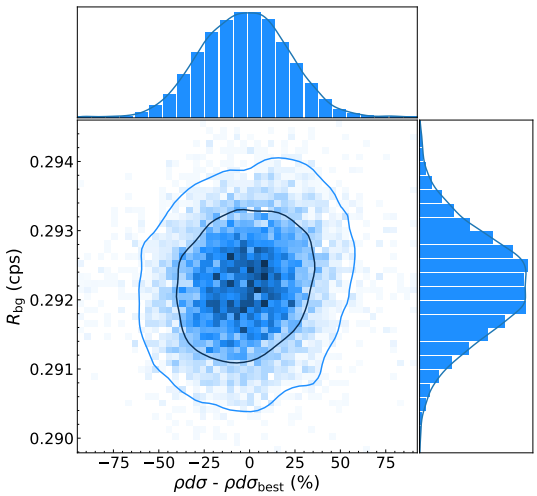

(c) Background rate R_{bg}

Figure 7.3: Scatter plot of fit values of ρdσ in combination with fit values of the endpoint E_0, the signal normalization A_S and the background rate R_{bg}. The error contours for the best fit point are displayed for 1-σ (black line) and 2-σ (blue line). A positive correlation of the column density with the endpoint and the normalization can be seen. The background and ρdσ show no correlation.

Chapter 8

Conclusion

In this work the method to determine the column density with the photo-electric source was presented and the successful application to the first neutrino mass measurement was shown. The response model of the e-gun electrons, that is a vital component of this method, was refined to include a realistic energy and angular distribution of the photo-electrons. To include systematic uncertainties in the response model fit, the Covariance Matrix approach was used and the relevant systematic contributions identified. The column density measurements taken with the electron gun during KNM-1 were analyzed and the ability to determine the column density with high precision using this method was verified.

A strategy to address the column density instabilities during the first neutrino mass measurement was co-developed and successfully used in the first neutrino mass analysis. To accomplish a continuous monitoring of the column density with high precision a combination of the measurement with the electron gun and the flowmeter sensor was used. This choice was based on a study of the stability of different column density monitoring devices. With this strategy the determination of $\rho d\sigma$ during the first neutrino mass measurement could be established with a relative uncertainty of less then 0.85 %.

To reduce the amount of measurement time, that is needed for a precise determination of $\rho d\sigma$ with the e-gun a study based on Monte Carlo generated data was performed. Two different settings of the KATRIN experiment were addressed and an optimized measurement time distribution for both settings was found. This optimization was applied in the measurements with the electron gun during KNM-1.

Information about the column density is imprinted in the integral β-spectrum, that is measured by the KATRIN experiment. By setting $\rho d\sigma$ as a free parameter in the neutrino mass fit its value could be studied from the tritium spectra itself. For large fit ranges, which are most sensitive to the column density, a good agreement with the $\rho d\sigma$ result, obtained via e-gun calibration, was obtained. Setting the column density as a free parameter allowed the study of the correlation with the other fit parameters.

As a result this work showed that the determination of the column density with high precision, that is needed for the goal of the KATRIN experiment to measure m_ν with a sensitivity of 200 meV, can be achieved by performing measurements with the e-gun and continuous monitoring devices.

Bibliography

[AAA+02] Q. R. Ahmad, R. C. Allen, T. C. Andersen, et al. "Direct Evidence for Neutrino Flavor Transformation from Neutral-Current Interactions in the Sudbury Neutrino Observatory". In: *Phys. Rev. Lett., 89:011301* (2002). URL: https://arxiv.org/abs/nucl-ex/0204008v2.

[AAA+19] M. Aker, K. Altenmüller, M. Arenz, et al. "Improved Upper Limit on the Neutrino Mass from a Direct Kinematic Method by KATRIN". In: *Physical Review Letters* 123.22 (2019). ISSN: 1079-7114. DOI: 10.1103/physrevlett.123.221802. URL: http://dx.doi.org/10.1103/PhysRevLett.123.221802.

[AAB+05] J. Angrik, T. Armbrust, A. Beglarian, et al. *KATRIN Design Report 2004*. Tech. rep. Forschungszentrum Karlsruhe, 2005. URL: https://publikationen.bibliothek.kit.edu/270060419.

[ABB+11] V. N. Aseev, A. I. Belesev, E. V. Berlev, et al. "An upper limit on electron antineutrino mass from Troitsk experiment". In: *Phys. Rev. D 84 (2011) 112003* (2011). URL: https://arxiv.org/abs/1108.5034.

[ABB+15] J. F. Amsbaugh, J. Barrett, A. Beglarian, et al. "Focal-plance detector system for the KATRIN experiment". In: *Nucl. Inst. Meth. A 778 (2015) 40-60* (2015). URL: https://arxiv.org/abs/1404.2925.

[Agh+18] N. Aghanim et al. *Planck 2018 results. VI. Cosmological parameters*. 2018. arXiv: 1807.06209 [astro-ph.CO].

[Ake+19] M. Aker et al. *First operation of the KATRIN experiment with tritium*. 2019. arXiv: 1909.06069 [physics.ins-det].

[Are+18] M. Arenz et al. "First transmission of electrons and ions through the KATRIN beamline". In: *Journal of Instrumentation* 13.04 (2018), P04020–P04020. ISSN: 1748-0221. DOI: 10.1088/1748-0221/13/04/p04020. URL: http://dx.doi.org/10.1088/1748-0221/13/04/P04020.

[Bab14] M. Babutzka. "Design and development for the Rearsection of the KATRIN experiment". PhD thesis. Karlsruhe Institut für Technologie, 2014. URL: https://publikationen.bibliothek.kit.edu/1000045598.

[Bar18] A. S. Barabash. *Main features of detectors and isotopes to investigate double beta decay with increased sensitivity*. 2018. arXiv: 1803.06894 [nucl-ex].

[Beh16] J. Behrens. "Design and commissioning of a mono-energetic photoelectron source and active background reduction by magnetic pulse at the KATRIN experiment". PhD thesis. Westfälische Wilhelms-Universität Münster, 2016. URL: https://www.katrin.kit.edu/publikationen/phd_behrens.pdf.

[Blo] F. Block. "In Preparation". PhD thesis. Karslruhe Institut für Technologie.

[BPT80] G. Beamson, H. Q. Porter, and D. W. Turner. "The collimating and magnifying properties of a superconducting field photoelectron spectrometer". In: *J. Phys. E: Sci. Instrum., 13:64* (1980). URL: https://iopscience.iop.org/article/10.1088/0022-3735/13/1/018/pdf.

[BS64a] C. N. Berglund and W. E. Spicer. "Photoemission Studies of Copper and Silver: Experiment". In: *Phys. Rev.* 136 (4A 1964), A1044–A1064. DOI: 10.1103/PhysRev.136.A1044. URL: https://link.aps.org/doi/10.1103/PhysRev.136.A1044.

[BS64b] C. N. Berglund and W. E. Spicer. "Photoemission Studies of Copper and Silver: Theory". In: *Phys. Rev.* 136 (4A 1964), A1030–A1044. DOI: 10.1103/PhysRev.136.A1030. URL: https://link.aps.org/doi/10.1103/PhysRev.136.A1030.

[CDD+98] B. T. Cleveland, T. Daily, R. Davis, et al. "Measurement of the Solar Electron Neutrino Flux with the Homestake Chlorine Detector". In: (1998). URL: https://iopscience.iop.org/article/10.1086/305343.

[Cha14] J. Chadwick. "Intensitätsverteilung im magnetischen Spectrum der β-Strahlen von radium B + C". In: *Verhandlungen der Deutschen Physikalischen Gesellschaft, 16:383-391* (1914). URL: http://cds.cern.ch/record/262756.

[CRH+56] C. L. Cowan, F. Reines, F. B. Harrison, et al. "Detection of the Free Neutrino: a Confirmation". In: *Science, 124(3212):103-104* (1956). URL: https://science.sciencemag.org/content/124/3212/103.

[Fer34] E. Fermi. "Versuch einer Theorie der β-Strahlen". In: *Zeitschrift für Physik, 88(3-4):161-177* (1934). URL: https://link.springer.com/article/10.1007/BF01351864.

[FHI+98] Y. Fukuda, T. Hayakawa, E. Ichihara, et al. "Evidence for oscillation of atmospheric neutrinos". In: *Phys. Rev. Lett., 81:1562-1567* (1998). URL: https://arxiv.org/abs/hep-ex/9807003v2.

[Fow31] R. H. Fowler. "The Analysis of Photoelectric Sensitivity Curves for Clean Metals at Various Temperatures". In: *Phys. Rev.* 38 (1 1931), pp. 45–56. DOI: 10.1103/PhysRev.38.45. URL: https://link.aps.org/doi/10.1103/PhysRev.38.45.

[GB76] M.L. Glasser and A. Bagchi. "Theories of photoemission from metal surfaces". In: *Progress in Surface Science* 7.3 (1976), pp. 113–148. ISSN: 0079-6816. DOI: https://doi.org/10.1016/0079-6816(76)90003-4. URL: http://www.sciencedirect.com/science/article/pii/0079681676900034.

[GP12] A. Giuliani and A. Poves. "Neutrinoless Double-Beta Decay". In: (2012). URL: http://dx.doi.org/10.1155/2012/857016.

[Ha17] Florian Heizmann and Hendrik Seitz-Moskaliuk and. "The Windowless Gaseous Tritium Source (WGTS) of the KATRIN experiment". In: *Journal of Physics: Conference Series* 888 (2017), p. 012071. DOI: 10.1088/1742-6596/888/1/012071. URL: https://doi.org/10.1088%2F1742-6596%2F888%2F1%2F012071.

[HW97] J. R. M. Hosking and James R. Wallis. *Regional Frequency Analysis: An Approach Based on L-Moments*. Cambridge University Press, 1997. DOI: 10.1017/CBO9780511529443.

[Jan15] A. Jansen. "The Cryogenic Pumping Section of the KATRIN Experiment - Design Studies and Experiments for the Commissioning". PhD thesis. Institut für Experimentelle Kernphysik, KIT, 2015. URL: https://publikationen.bibliothek.kit.edu/1000047146.

[Kar18] C Karl. "Analysis of First Tritium Data of the KATRIN Experiment". MA thesis. Technical University of Munich, 2018. URL: https://www.katrin.kit.edu/publikationen/mth-karl.pdf.

[KBB+05] Ch Kraus, B. Bornschein, L. Bornschein, et al. "Final results from phase II of the Mainz neutrino mass searchin tritium β decay". In: *Eur. Phys. J. C 40, 447–468 (2005)* (2005). URL: https://link.springer.com/article/10.1140/epjc/s2005-02139-7.

[KBD+19] M. Kleesiek, J. Behrens, G. Drexlin, et al. "β-Decay spectrum, response function and statistical model for neutrino mass measurements with the KATRIN experiment". In: *The European Physical Journal C* 79.3 (2019). ISSN: 1434-6052. DOI: 10.1140/epjc/s10052-019-6686-7. URL: http://dx.doi.org/10.1140/epjc/s10052-019-6686-7.

[Kuc16] L. Kuckert. "The Windowless Gaseous Tritium Source of the KATRIN Experiment - Characterisation of Gas Dynamical and Plasma Properties". 51.03.01; LK 01. PhD thesis. Karlsruher Institut für Technologie (KIT), 2016. DOI: 10.5445/IR/1000065077.

[Liu87] J. W. Liu. "Total cross sections for high-energy electron scattering by H_2 ($^1\Sigma_g^+$), N_2 ($^1\Sigma_g^+$), and O_2 ($^3\Sigma_g^-$)". In: *Phys. Rev. A., 35:591* (1987). URL: https://journals.aps.org/pra/pdf/10.1103/PhysRevA.35.591.

[LS85] V. M. Lobashev and P. E. Spivak. "A METHOD FOR MEASURING THE ANTI-ELECTRON-NEUTRINO REST MASS". In: *Nucl. Instrum. Meth.* A240 (1985), pp. 305–310. DOI: 10.1016/0168-9002(85)90640-0.

[Mar] A. Marsteller. "In Preparation". PhD thesis. Karslruhe Institut für Technologie.

[Mar17] A Marsteller. "Measurement of Temperature Stability andHomogeneity of the KATRIN WGTSCryostat". MA thesis. Karlsruhe Institut für Technologie (KIT), 2017. URL: https://www.katrin.kit.edu/publikationen/mth_marsteller.pdf.

[MNS62] Z. Maki, M. Nakagawa, and S. Sakata. "Remarks on the unified model of elementary particle". In: (1962). URL: https://academic.oup.com/ptp/article/28/5/870/1858382.

[MWH98] M. Matsuyama, K. Watanabe, and K. Hasegawa. "Tritium assay in materials by the bremsstrahlung counting method". In: *Fusion Engineering and Design* 39-40 (1998), pp. 929–936. ISSN: 0920-3796. DOI: https://doi.org/10.1016/S0920-3796(98)00232-4. URL: http://www.sciencedirect.com/science/article/pii/S0920379698002324.

[OW08] E. W. Otten and C. Weinheimer. "Neutrino mass limit from tritium β decay". In: *Reports on Progress in Physics* 71.8 (2008), p. 086201. DOI: 10.1088/0034-4885/71/8/086201. URL: https://doi.org/10.1088%2F0034-4885%2F71%2F8%2F086201.

[Pau30] W. Pauli. "Offener Brief an die Gruppe der Radioaktiven bei der Gauvereins-Tagung zu Tübingen". 1930. URL: https://cds.cern.ch/record/83282.

[PB02] Z. Pei and C. N. Berglund. "Angular Distribution of Photoemission from Gold Thin Films". In: *Japanese Journal of Applied Physics* 41.Part 2, No. 1A/B (2002), pp. L52–L54. DOI: 10.1143/jjap.41.l52. URL: https://doi.org/10.1143%2Fjjap.41.l52.

[PBB+92] A. Picard, H. Backe, H. Barth, et al. "A solenoid retarding spectrometer with high resolution and transmission for keV electrons". In: *Nuclear Instruments and Methods in Physics Research Section B: Beam Interactions with Materials and Atoms* 63.3 (1992), pp. 345–358. ISSN: 0168-583X. DOI: https://doi.org/10.1016/0168-583X(92)95119-C. URL: http://www.sciencedirect.com/science/article/pii/0168583X9295119C.

[Pon68] B. Pontecorvo. "Neutrino experiments and the problem of conservation of leptonic charge". In: (1968). URL: http://inspirehep.net/record/51319?ln=de.

[Pov+15] B. Povh et al. *Particles and Nulcei*. Springer, 2015. URL: https://www.springer.com/de/book/9783662463208.

[Röl15] M. Röllig. "Tritium analytics by beta induced X-ray spectrometry". PhD thesis. Karlsruhe Institut für Technologie, 2015. URL: https://publikationen.bibliothek.kit.edu/1000054050.

[Sch19] L Schlüter. "Development of New Methods to Include Systematic Effects in the First Tritium Data Analysis and Sensitivity Studies of the KATRIN Experiment". MA thesis. Technical University of Munich, 2019. URL: https://www.katrin.kit.edu/publikationen/SchlueterLisaMSc19%20(1).pdf.

[Wal13] B. L. Wall. "Karlsruhe Tritium Experiment: Detector System Commissioning and In-Situ PIN-Diode Array Dead-Layer Measurement". PhD thesis. University of Washington, 2013. URL: https://digital.lib.washington.edu/researchworks/handle/1773/22845.

[Zac14] M. Zacher. "High-field electrodes design and an angular-selective photoelectron source for the KATRIN spectrometers". PhD thesis. Westfälische Wilhelms-Universität Münster, 2014.

[Zub11] K. Zuber. *Neutrino Physics*. CRC Press, 2011. URL: https://www.crcpress.com/Neutrino-Physics/Zuber/p/book/9781420064711.

Acknowledgements

In the end, I would like to thank all the people who supported me during my masther's thesis. In particular:

- Prof. Dr. Susanne Mertens for giving me the opportunity to work on this thesis in this exciting phase of the KATRIN experiment, the constant support and the many interesting and fruitful discussions,
- Christian Karl for his outstanding supervision and the many helpful discussions concerning all Fitrium and physics related topics,
- Fabian Block and Alexander Marsteller for the great teamwork in the column density task force, that lead to numerous extensive and constructive discussions,
- Dr. Thierry Lassere for his helpful comments on the column density subject,
- Dr. Martin Slezák for fruitful discussions on Fitrium and physics related topics,
- Dr. Jan Behrens and Lutz Schmipf for providing me with detailed knowledge about the photo-electron source,
- Dr. Alexey Lokhov for his helpful introduction into Kasper,
- Manuel Lebert, Matthias Meier and Korbinian Urban for making our shared office a special place,
- the whole Munich KATRIN/TRISTAN group for the wonderful working atmosphere and the many activities in and outside of physics,
- the KATRIN collaboration for the warm welcome and the opportunity to be a part of this experiment,

and especially my family and friends for their permanent support and encouragement.